NASA-CR-195772

0

55 p

Correlation Studies of Pioneer Venus Imagery Obtained from PV Experiments with Near-IR Imagery Obtained from Ground-Based Observations during Venus Inferior Conjunction

NASA-Ames Research Center
Research Grant Number
NAG 2-681

Final Report

October, 1993

Jindra Goodman, Project Director
Boris Ragent, Principal Investigator

San Jose State University Foundation
One Washington Square
San Jose, California, 95192-0139

Correlation Studies of Pioneer Venus Imagery Obtained from PV Experiments with Near-IR Imagery Obtained from Ground-Based Observations during Venus Inferior Conjunction

I. Introduction

Data taken by instruments aboard the Pioneer-Venus Orbiter (PVO) over its lifetime provided a unique time series of measurements which have been extremely useful in helping to describe the behavior of the upper atmosphere of Venus (Mutch, 1980; Hunten et al., 1983). However, much of the data taken by some of these instruments, for example, the Cloud Photopolarimeter (OCPP), have not been analyzed in detail, since in the past many of the principal results of these experiments were achieved by considering only portions of the available data, or because it was considered that no further useful analyses could be performed at that time.

During short periods near inferior conjunction over about the past ten years, Earth-based near-infrared (NIR) measurements of the dark side of Venus have been obtained. The results of these measurements have indicated that there are spectral atmospheric "windows" for radiation propagating through the atmosphere, and that the clouds in the middle atmosphere have much inhomogeneous structure associated with them, structure that can be used to study atmospheric motion and wave properties (Allen and Crawford, 1984; Crisp et al., 1989, 1991a, 1991b; Kamp et al., 1989; Kamp and Taylor, 1990; Allen et al., 1992). Spectral atmospheric "windows" centered at wavelengths as short as about 1.0 micron have been found to exist, and measurements made in these shorter wavelength windows have shown that radiation propagating from the planetary surface all the way through the atmosphere may be observed. These observations have raised the question as to whether any of the partially-analyzed available data, from say the OCPP 0.935 micron channel, may be used for similar further atmospheric and cloud studies.

PVO measurements, especially those recording radiation received from the solar illuminated portions of the planet at short wavelengths, say, for example, 0.365 microns for one of the OCPP channels, have been extensively used to document the upper atmospheric cloud structure and motion, from which descriptions of atmospheric motion and waves have been derived (Rossow et al., 1980, 1990; Schubert, 1983; Limaye, 1984). Contrast ratios for cloud features, even for data at these ultraviolet (UV) wavelengths are small, usually less than 10 percent. Data obtained at longer wavelengths, for example in the visible, has, in the past, not shown contrast ratios that were large enough to produce useful imagery. However, since such positive results have been obtained from the Earth-based NIR experiments, it is imperative that the PVO data be reexamined, especially solar

illuminated OCPP 0.935 micron channel data, even though they may indicate very low contrast features. The need for extreme care in processing such low contrast data, and in making necessary corrections in order to unambiguously identify such features, is obvious.

The purpose of this study is to attempt to find correlations between data taken by experiments aboard the Pioneer-Venus Orbiter (PVO) and those obtained from Earth-based near-infrared (NIR) measurements of Venus during periods near inferior conjunction. Since the NIR measurements have been found to provide data on the middle atmosphere cloud morphology and motion, it is assumed that any correlations will also indicate that the PVO experiments are also documenting cloud behavior. If such correlations are found, then a further task is to attempt to study the long term behavior of the cloud features implied by the correlations. Many PVO data have been obtained over an extended period extending from 1978 until the PV demise in 1992. There exists a long, somewhat ill-conditioned time series of data that may contain valuable information on the long time, as well as short term behavior of the clouds, and, derivatively from cloud motion, atmospheric dynamics and wave activity in the Venus atmosphere. For example, determination of the zonal velocities of any OCPP 0.935 micron features could then be used for comparisons with data from other sources to attempt to fix the altitude region in which such features existed. A further task of this study is to attempt to correlate any features found in simultaneously obtained data, for example, the OCPP 0.365 and 0.935 micron data. The existence of such correlations may imply that data was obtained in overlapping altitude regions of the atmosphere.

Recent progress in processing radio-occultation data received from the PVO so as to produce accurate altitude profiles of temperature, and profiles of S and X band absorptivity from which concentrations of sulfuric acid vapor may be derived (Fjeldbo et al., 1971; Fahd and Steffes, 1992; Steffes, 1985, 1991; Jenkins, 1991, 1992a, 1992b), also suggested a further task. This involved attempting to obtain near simultaneous PV radio-occultation data and Earth-based NIR imagery during a period near inferior conjunction in September, 1991. These data were to be used to attempt to establish whether the large particles in the lower clouds that are, apparently, a principle contributor to the opacities present in the NIR data, are composed of sulfuric acid or some other material.

Although considerable progress was made in accomplishing the desired tasks of this study, not all of the desired goals were achieved during the time period of the study. Work along these directions is, however, proceeding under other auspices, with completion anticipated by mid 1994. In this study we have concentrated on studying (a) correlations of data available from the PVO OCPP instrument operated in its "polarimetry" mode, since these data appear to be most comparable with those from Earth-based NIR measurements, and (b) the results of comparing

atmospheric property altitude profiles obtained from radio-occultation data with nearly simultaneously obtained NIR data. The following sections contain discussions of the nature of the data, processing of the data, and present typical examples. Available NIR data are presented and initial correlations are discussed. A discussion of tentative results and conclusions, work remaining, and future activities is presented.

II. Processing and Correlation of PV OCPP and Earth-Based NIR Data.

A. Data for Periods Near Inferior Conjunctions of January, 1990, and June, 1988.

1. General Description

Our initial activities involved attempting to process and analyze the PV OCPP data and Earth-based NIR images of the dark side of Venus obtained during the period preceding and following the conjunction of January 18, 1990, as well as some of those obtained in May and June of 1988. Most of the pertinent data recorded by the OCPP experiment aboard the PVO during these periods and necessary ancillary descriptive data such as times, applicable angles, latitudes and longitudes, etc. for each data point, were obtained from Larry Travis, Principal Investigator for the OCPP, and our collaborator. These data had to be converted into the "FITS" format presently used by most astronomical investigators, to match available processing programs. The NIR data were available from data banks collected by David Crisp and Boris Ragent including, in large part, data derived from observations performed by these investigators and their collaborators.

2. Processing of OCPP Data

The OCPP data require extensive treatment to retrieve the features in which we are interested. The signal recorded by the OCPP in its "polarimetry" mode is composed of sunlight scattered into the OCPP by the atmosphere and its particulate matter. The signal, due to scattering of incident sunlight in the atmosphere and clouds into the field of view of the OCPP instrument, is composed primarily of a large component that varies smoothly with changes of the observing solar zenith and observation zenith angles, and that shows the very strong influence of limb-darkening. The signal also contains a very low contrast, small, variable component produced by modulation in the scattering of the sunlight by inhomogeneities in the atmosphere or clouds. It is this small component due to the inhomogenieties that is of principle concern and interest in this study, and it is necessary to attempt to extract it from the OCPP data.

Two general approaches have been attempted for processing the OCPP data. One attempt, developed by Travis, includes attempting to calculate the amount of scattered light, including multiple

scattering, from a uniformly stratified atmosphere with no horizontal inhomogeneities, using a model of cloud structure and atmosphere obtained from "standard" cloud and atmosphere descriptions. OCPP signal values that would be recorded for these calculated scattered light values are obtained by normalization with a measured datum point (for example, by normalizing the maximum calculated scattered light value with the maximum measured data value), or by using the calibrated values of detector sensitivities. The values of the signals derived from the calculations for each instrument viewing configuration are then subtracted from the actual OCPP measured values to obtain the spatially varying contribution. The program and calculational procedures used for this approach are described in Appendix A.

A second approach, also previously used by Limaye and associates for analyzing OCPP data (Limaye, 1984), involves using a technique originally proposed by Minnaert for studying the light scattered from the surfaces of solid objects in the solar system. The implied assumption of this method is that the detailed scattering from inhomogeneities in the atmosphere resembles essentially that from a diffusely scattering solid target, so that the scattered radiation from a given differential element of scattering area is almost independent of the angle of observation. The function expressing the relationship among the pertinent quantities may be written,

$$I = A\,\mu_c^{k}\,\mu^{k-1} \qquad (1)$$

or,

$$\ln(\mu I) = \ln A + k \ln(\mu\mu_o) \qquad (2)$$

where,

I = scattered intensity
$\mu = \cos\theta$
$\mu_o = \cos\theta_o$
θ = the observer zenith angle
θ_o = the solar zenith angle
k = an exponent approximately equal to one
A = a constant, equal to I when $\mu = \mu_o = 1$

The measured data, Im, and associated values of μ and μ_c, are used to calculate a straight line least squares fit for $\ln(\mu Im)$ as a function of $\ln(\mu\mu_o)$ in order to determine A and k. The A and k, thus found, are used to calculate values of I for the μ and μ_o of each measured data point. The I are then subtracted from Im to obtain Id, the values of the the measured intensity that vary from the expected mean. These are the values used to characterize the inhomogeneous scattering, and, assumedly, cloud or atmospheric nonuniformities. A typical plot of measured 0.365 micron data plotted in the form of $\ln(I\mu)$ versus $\ln(\mu\mu_o)$ is shown in Figure 1a. A similar plot prepared using 0.935 micron data

recorded almost simultaneously with the 0.365 micron data used in Figure 1a is shown in Figure 1b. The lines for the least squares fits to the data are also plotted in these figures. In fitting these lines to calculate values for A and k, it has been found that certain types of features are better displayed in the imagery if data for restricted values of ln ($\mu\mu_0$), that is, only data for restricted values of the product of the cosines of the solar zenith angle and observer zenith angles, are used in the least squares fitting. Plots limiting the data used to those for values of ln ($\mu\mu_0$) > -2.5 are shown in Figures 1c and 1d.

There are characteristic features in these plots that, obviously, reflect characteristic features in the images formed from these data. The general external contour of the data for 0.365 microns shown in Figure 1a exhibits a pointed "nose", a bird-like head, followed by a contained, but expanding body. Within this outlined shape are a number of arc-shaped structures, and, below it a number of points appearing to form a curved shape dropping from the main body of points. Similar behavior is evident in plots of earlier data by other investigators (Limaye et al., 1984).

The shape of the outlines of the data for 0.365 microns shown in Figure 1a appears to be much more detailed than that for the 0.935 micron data shown in Figure 1b, and the data appear to be much closer to the fitted least sqares line, showing the much smaller range of contrasts present for the features at the longer wavelength. There are, however, some less evident characteristics in each of the plots of these data that stongly resemble each other, and, appear at the same values of ln ($\mu\mu_0$) in both plots. Some of these features are marked with arrows in the two plots. The similarities of these features and their location at the same places on the plots stongly implies that the data collected at both wavelengths are from the same "object" in their field of view, and, probably, from a cloud feature at an altitude accessible to both measurements, i. e., at an overlapping sampled altitude range. As yet, these common features have proven to be difficult to identify in the actual images formed from the data.

Since it takes the OCPP instrument about four hours to build up a point by point image, a further small correction to the longitude for each data point has been applied by assuming that the atmosphere is rotating from east to west with a fixed rotation period. Images formed from the same set of February 10, 1990, 0.935 micron, OCPP data, using the results of processing by the two approaches, are shown in Figures 2a and 2b. The assumed rotation period used in preparing these images was 5.5 days. Some enhancement (stretching) of the intensity scale in the images has been applied by subtraction of underlying intensities and expanding the variations of remaining intensities using a power law. An image of 0.365 micron OCPP data taken at the same time as the 0.935 micron images, and prepared with the "Minnaert" approach is shown in Figure 2c.

If it is assumed that the features in the atmosphere do not change rapidly compared with periods between successive data sets, and that these features are rotating with the atmosphere, then images prepared from data taken during succeeding time periods may be combined into a mosaic. The principle assumption in preparing such a mosaic is that the mosaic, prepared using data obtained for different latitude-longitude regions in the atmosphere at different times over an extended period, say, perhaps a week, is essentially the same as would have been obtained if all of the data for these different regions had been obtained at the same time. Mosaics prepared with OCPP data obtained during February, 1990, and using the "Minnaert" approach for several assumed atmospheric rotation periods are shown in Figures 3a, 3b and 3c. The actual presence and shapes of features are best confirmed from their appearance in successive images. The motion of features recognizably present in images prepared from successive OCPP data sets may be directly measured. Unfortunately, in the mosaics shown in Figure 3, the time periods, and even gaps, between successive images were too large to permit accurate measurements of feature velocities to be made easily. However, the apparent fitting together of different features in successive images for each of the two assumed rotation periods suggests that in any image there may be features moving with differing velocities, perhaps similar to those found in the NIR imagery (see, for example, Crisp et al., 1991b; Carlson et al., 1991). A series of images from data obtained with much shorter time separations in June, 1988 is now (October, 1993) being prepared, and promises to allow much better feature definition and more accurate documentation of feature velocities (Yee and Ragent, in preparation).

3. Processing of Earth-Based NIR Data

In preparing and processing Earth-based NIR data initial attention was directed to the data for periods near inferior conjunction in 1988, 1990 and 1991, periods for which fairly good NIR data sets exist, and, especially for those periods for which, it was thought, data from the PV OCPP experiment was also available. The NIR data, taken at a number of observatories by a number of investigators, many of whom are involved with this study, have previously been presented (Crisp et al, 1989; Crisp, 1990a, 1990b; Crisp et al 1991a, 1991b; Sinton et al., 1990; Ragent et al., 1990; Kalas and Ragent, 1992). Examples of the 1990 images are shown in Figure 4. Descriptions of the general techniques for processing these types of data have been presented (McCaughean, 1989). The processing involves considerations of sky background, array detector pixel sensitivities, linearities, noise, addition of images, etc.. Scattering from the bright crescent must be removed by subtraction, using images obtained in spectral regions outside the atmospheric windows in which the principal NIR images were obtained. Limb darkening effects are taken into account using preferred algorithms. In addition, cylindrical projections of the disk images onto a latitude-

longitude grid are then prepared, making corrections in each image for pixel dimensional distortions. The projections are prepared by first accurately locating the coordinates of the center of the disk of each image, tagging this point with the sub-Earth point coordinates for that time, establishing geographical directional coordinates for each image, and then establishing a latitude-longitude coordinate system onto which to project each pixel in the raw data. Smoothing of the data is often used, applying any of a number of various approaches. The cylindrical projections of images taken in time sequence over a sufficient time period may be combined into a mosaic of the entire planet, using the assumption, as previously done for the PV OCPP, that the features present in the images do not dissipate quickly, and that the atmosphere rotates zonally with a fixed rotation period. Examples of mosaics of NIR measurements made in two periods from December 31 to January 7,1990 and from February 7, 1990 through February 15, 1990 are shown in Figure 5. Feature velocities can also be measured from successive images (Crisp et al., 1991b; Carlson et al., 1991), and a typical plot of these velocities is shown in Figure 6.

B. Correlation of PV OCPP and NIR Data

A general program for establishing correlations among features common to two images projected onto latitude-longitude coordinates has been written, and is documented in detail in Appendix B. In essence the program reads the latitude-longitude maps of the planet obtained at different times, and finds feature rotation rates by shifting the maps in longitude, finding the root-mean-square and absolute value of the difference between the maps at each position. It defines the longitude shift that gives the smallest rms or absolute difference in each longitude bin as the choice for best fit. It then finds the rotation rate and zonal velocity corresponding to that shift. The regions of investigation and other required quantities are chosen by (1) choosing the sizes for a latitude-longitude patch or box to be used, (2) the number of pixels to be scanned in latitude and longitude for a given latitude-longitude box, (3) the minimum fraction of the number of pixels that must overlap for a valid velocity measurement, (4) the minimum fraction of variance in the reference box that must be accounted for at the position of best alignment, (5) the minimum fractional rms within a box to establish that it includes one or more features, (6) the maximum uncertainty in wind velocity that is reported (if the uncertainty is greater than the specified maximum error the wind velocity is not reported), (7) the specified maximum error in wind velocity that is reported, and (8) the time difference between images 1 and 2, the FITS formatted latitude-longitude projected images to be correlated.

Our original choice for comparing OCPP and NIR imagery was to use the data obtained during periods near the 1990 inferior conjunction. This choice was based on the fairly extensive NIR data available from a well coordinated observational effort, and

even included data obtained during the Galileo Mission encounter with Venus in February, 1990. Again, unfortunately, as described above, after processing of the data it developed that relatively sparse good OCPP imagery was available for this period. Using the mosaic of the most suitable 1990 OCPP observations, Figure 3, it proved to be difficult to correlate the features shown in it with those present in the Figure 5 1990 NIR mosaic made from data obtained during nearly the same time period (displaced in longitude, of course, to account for the different portions of the globe viewed simultaneously by the OCPP and NIR experiments). Tantalizing hints, and perhaps even more definite indications of such correlations, appear to be present, but they are too indefinite, as yet, to draw any conclusions. As mentioned above the work now in progress to prepare the much more extensive 1988 OCPP data set promises to make available a much better comparison (Yee and Ragent, in preparation).

III. Correlation of Radio-Occultation and Nearly Simultaneous NIR Measurements Obtained During a Period Near Inferior Conjunction in September, 1991.

A. General Purpose and Concept

The clouds of Venus are composed of particles of several size modes. There is substantial agreement that the smaller size mode paricles are composed principally of sulfuric acid. However, the composition of the largest particles, found principally in the lower and lower-middle cloud regions, is still uncertain, and is the subject of ongoing discussion (see, for example Toon et al., 1984; Knollenberg, 1984). In particular, there is a question as to whether these particles are liquid droplets, presumably also largely composed of sulfuric acid, or solid particles composed of other species.

Several observational results have strongly suggested that the concentration of these large mode particles is spatially inhomogeneous, and varies greatly, temporally and geographically, over the planet, probably as a result of atmospheric dynamical effects (Ragent et al., 1987, Crisp et al., 1989, 1991b, Carlsen et al., 1991, 1993). The features evident in the NIR images of the dark side of Venus have been attributed to inhomogeneities in the lower and the lower-middle cloud structures, almost certainly associated with variations in the concentration of large particles. Thus regions of higher NIR transmission are thought to reflect a smaller large particle population. If the particles are indeed composed of sulfuric acid, than their absence, presumably due to evaporation, implies a higher sulfuric acid vapor concentration in these regions than in regions of denser large particle concentration.

Radio occultation experiments using radio signals transmitted from the PV Orbiter through the Venus atmosphere to Earth have yielded altitude profiles of both atmospheric temperature and absorptivity (Kliore and Patel, 1982; Steffes et al., 1991;

Jenkins and Steffes, 1991; Jenkins, 1992; Jenkins and Ragent, 1992). In recent years it has been shown that a principal absorber at these frequencies is sulfuric acid vapor, and profiles of sulfuric acid vapor concentrationhave been published (Jenkins and Steffes, 1991; Steffes et al., 1991; Jenkins, 1992; Jenkins and Ragent, 1992). This suggests that strong arguments about the composition of the large particles could be obtained by comparing nearly simultaneous determinations of altitude profiles of sulfuric acid vapor concentration, especially at altitudes just below the clouds, with measured NIR opacities in the same region of the planet. If the opacity variations are due to particle formation or destruction, then sulfuric acid vapor concentration profiles just below the clouds should be anti-correlated with cloud opacity.

As a result of these considerations we proposed, under this grant, that NIR images of the dark side of Venus be obtained during a period near the inferior conjunction of August 23, 1991, and that, since conditions for obtaining such data were favorable for that period, radio occultation data be obtained during the same period. Boris Ragent agreed to attempt to obtain the NIR data and Arvydas Kliore and Jon Jenkins assumed responsibility for the radio occultation efforts.

B. Earth-Based NIR Measurements of Venus in July and September of 1991.

1. Pre-Conjunction Measurements at Lick Observatory, July, 1991.

A proposal for telescope time at Lick Observatory of the University of California on Mount Hamilton, California was submitted, and, with the assistance of Professor David Rank and several graduate students, observations of Venus were attempted starting on July 22, 1981. Initial observations were begun at the 1 meter (40 inch) telescope, using the NICMOS camera (128x128 HgCdTe detector array, optics, filter wheel and cryogenics) of the Astronomy Department of the University of California at Santa Cruz. Unfortunately, after having to realign and perform a number of adjustments, it was found that the mounting did not allow sufficient depression of the telescope to allow viewing Venus for more than a few minutes after sunset. Because of very bad sky scattering conditions that made viewing after sunset essential, and the restricted viewing arrangement, no usable data was obtained on this night. We tried again on the succeeding night without success, considering the very short effective time available for viewing, and discovering additional difficulties in using the camera to view such a bright object. We tried a number of fixes with only modest results. Results obtained on the following night of July 24, 1991 were somewhat better, but the observations were not of high enough quality to permit the preparation of useful images.

On Thursday, July 25, 1991 the camera and equipment were moved and installed on the Lick 120 inch (3 meter) telescope.

Alignments were made and a gold attenuating filter (ND=2) was installed ahead of the camera. No data were obtained this night. The following night, after continuing to adjust and refine the apparatus, data were taken, but enormous amounts of sky background and light scattered internally in the telescope and camera badly reduced the effective quality of the data. A necessity to shorten the exposure time from the shortest time available on the camera became evident, without an easy timely fix possible. Data were also obtained the following night, attempting to use additional neutral density attenuators, with only very modest improvement.

In summary, no useful data were obtained from these observations, but much useful insight and advice was obtained on how to make measurements during the post-conjunction period scheduled during September, 1991.

2. Post Conjunction Observations, September, 1991.

Successful observations of the dark side of Venus were obtained at the "Air Force" 24 inch (0.6 meter) telescope of the University of Hawaii on Mauna Kea, Hawaii, on the mornings of September 14 through 21, 1991. The work was performed under the direction of Boris Ragent with the collaboration and support of Richard Wainscoat, Professor David Jewitt, Paul Kalas and several graduate students of the Institute for Astronomy of the University of Hawaii. A NICMOS camera with a 256x256 array of HgCdTe detector elements, a filter wheel, cryogenics, etc. was used. The days and nights of September 11-13 were used to remount the telescope so as to increase the depression capability, and to properly align and orient the equipment. Observations of calibration stars, noise, and various background signals preceded the measurements of Venus during the following eight successive mornings. Venus was available for observation for periods of somewhat less than one hour before sunrise, starting at about 4:15 am (1415 UT). As soon as the sun rose, sky scattering, from debris deposited in the stratosphere from the Mount Pinatubo volcanic eruption of the preceding summer, completely masked the desired Venus signals. Nevertheless, notwithstanding the large air masses through which the observations were made, significant imagery of Venus was obtained.

Figure 7 shows a composite of images for each day (Kalas and Ragent, 1992). These images were taken using a 2.36 micron filter, and have been processed by flat fielding, including treatment for sky radiation, noise and detector linearity, coadded to improve the signal to noise ratios, and corrected for internal scattering by subtraction of imagery obtained using spectral filters near, but outside of the 2.36 micron atmospheric window. Figure 8 shows a mosaic constructed from these images, using the same assumptions as were done for the cases of the OCPP imagery discussed above (Kalas and Ragent, 1992). This process for these images involved locating the center of each disk,

assigning coordinates to this point from published ephemeris tables, projecting the data for each pixel onto a cylindrical longitude-latitude grid, and then combining images, assuming a zonal atmospheric rotation rate. Results for a number of assumed rotation rates are shown in Figures 9a through 9h.

Atempts at observations were also made at Lick Observatory, on a number of the same days as those at Mauna Kea. Although much progress was achieved over the previous attempts in July, the difficulties in making these measurements at this installation were so severe that they precluded obtaining satisfactory data.

C. Radio Occultation Data

Only four radio occultation measurements were obtained for dates close to the post conjunction period during which the good September, 1991 NIR imagery discussed above. Data were obtained for the occultations of September 10, 12, 17 , and 19, 1991. The data have been analyzed by Jon Jenkins, our collaborator, using essentially the techniques described in Jenkins, 1992. Altitude profiles of atmospheric temperature, absorptivity, and sulfuric acid vapor concentration were derived. During the course of these analyses it was found that, unfortunately, the signal received by the DSN was so noisy that there were large uncertainties in the absorptivities and sulfuric acid vapor concentrations derived from the received data at the lower altitudes of interest here. It was found that, perhaps except for indicating trends, little significance could be attached to comparisons among the profiles at altitudes below about 50 km above the assumed planetary radius of 6052 km. The temperature profiles, however, derived from refractivity and hence from accurate Doppler shift measurements were of high quality. For example, a plot of the estimated standard deviation of temperature at various altitudes for the data from orbit 4661 given in Figure 10, shows typical standard deviations of a small fraction of a degree over most of the altitude range of interest here.

Derived profiles for these data are shown in Figures 11a, 11b and 11c. No uncertainty bars have been attached to the absorptivity profile, since, although these are known to be very large, exact estimates of their values are not easily obtained. These profiles are shown as derived, but should not be used to draw conclusions about possible differences among absorptivity and implied sulfuric acid vapor concentration profiles. In contrast, differences in the temperature profiles are dramatic, and are indicative of very different atmospheric behavioral modes at the locations and times documented by these profiles.

Plots of temperature profiles in the cloud regions are shown in Figure 11. The profile for orbit 4670 shows temperatures about 5 degrees greater than those for orbits 4661 and 4663 at all altitudes in these regions. A plot of temperature versus pressure for these data is given in Figure 12a. A similar plot,

for the data received from the flight of the two balloons of the 1985 Vega Mission (Linkin et al., 1986) is also given in Figure 12b. The two balloons were inserted into the Venus atmosphere with a two day time period of separation. The similarity of these two plots in Figures 12a and 12b, made for data taken six years apart, is remarkable. This type of behavior can only be attributed to having sampled air masses of differing properties, probably caused by the propagation of characteristic, planetary, very long wavelength waves. Such profiles must also affect the cloud structure, as discussed in the next section. The temperature differences between the temperature profiles as presented in Figure 11 are evident, and profiles of plots of the density differences between the density profile for each orbit and that of the "standard" density profile (Seiff, 1983) are shown in Figure 13. The striking differences between the plots for orbit 4670 and the other orbits are readily apparent.

Altitude profiles of temperature residuals obtained by applying essentially high pass filtering techniques to these data are shown in Figures 14a, 14b and 14c.. These profiles show the detailed small scale structure of the temperature profile after the removal of the underlying smooth variation with altitude. Here again the large differences among the data from various orbits is strikingly displayed. Although this may be a coincidence, the data in Figure 14c show the profile for orbit 4670 almost appearing to follow the boundaries of the various cloud layers, perhaps implying a well defined cloud structure at the position of the profile. The profiles for the other three orbits in this Figure do not appear to be as well correlated with typical cloud structure. Residuals in temperature and density resulting from further filtering to eliminate lower frequency effects are shown in Figure 14a and 14b. The detailed shapes for the various orbits strongly suggest the presence of a pervasive, complicated, atmospheric wave structure at all of the altitudes sampled.

D. Correlations of Earth-Based NIR Imagery and Radio Occultation Results.

The latitude-longitude NIR mosaics shown in Figure 9b also contain symbols indicating the calculated effective locations of the radio occultation profiles presented in Figure 11. These locations have been derived by first locating the effective coordinates of the profiles at the actual times and dates of transmission. The longitude coordinate for each profile is then effectively rotated to accord with the elapsed time difference between the profile time and date and the reference time and date of the NIR mosaic, assuming the zonal atmospheric rotation rate to the west used for the mosaic. The assumption here, similar to that used in preparing the NIR mosaic, is that the profiles would remain essentially unchanged over the time differences used for relocating them onto the mosaic. From our previous experience in preparing mosaics from NIR data, it is believed that this is a reasonable assumption (for the effective altitudes at which the

opacity features exist) for periods of up to at least seven days for the largest opacity features present, but may only be valid for more a much shorter time for smaller features. The persistency of the profiles must be carefully considered in attempting to draw conclusions about correlations between the NIR opacities and the atmospheric property profiles derived from radio occultaions.

The four radio occultation profiles noted in Figure 9 were obtained on September 10, 12, 17, and 19, 1991, corresponding to PV orbits 4661, 4663, 4668, and 4670, respectively. The observations from which the NIR mosaic was constructed were made on September 14 through 21, 1991. The time differences for these data, although approximately meeting the criterion, suggested above, may not be short enough to allow firm conclusions about comparisons with NIR opacities for all of the profiles.

As mentioned above, there is a striking difference in the temperatures profiles shown in Figure 11 for orbit 4670 and the others. The opacity at the locations for the profile for orbit 4670, as shown in Figure 9b, also appears to be greater than the opacities at the locations of the other profiles. Such behavior, if real, is in not in accord with the hypothesis that the higher temperatures have led to appreciable evaporation of the larger particles in the clouds. Unfortunately, the accuracies of the absorptivity and derived sulfuric acid vapor profiles for the different orbits are not sufficient to be able to show a definite relationship with opacities. In addition, the magnitudes of the NIR opacities are not distinctive enough at all of the occultation profile locations to allow definite comparisons with each other. Hence, at least for the present, until better analyses or data are available, we cannot make any statement as to implications for the composition of the evaporating particles.

The discussion above, based on the somewhat sparse occultation data available from the PV Orbiter during the inferior conjunction period in 1991, has, however, shown that, with adequate and properly resolved data, very valuable insights into the clouds and atmospheric motions may be obtained from comparisons of NIR and radio occultation measurements. The occultation season in the summer and early fall of 1994, near inferior conjunction, will provide an ideal opportunity to obtain such data from the Magellan mission spacecraft, if available.

IV. Discussion and Conclusions

In this study we began an investigation of the use of some Pioneer-Venus Orbiter experiments data sets to further examine the properties of the Venus atmosphere. In particular correlations within OCPP data sets, of OCPP data sets with Earth-based NIR data sets, and of radio occultation data sets with Earth-based NIR data sets were examined. The object of these correlation studies is to establish the connection of the PVO

data sets with physical phenomena in the Venus atmosphere. If such relationships are established, then these types of PVO data, obtained over the 14 year period of PVO activity, will be useful in creating a long time series of measurements with which to model Venus atmospheric behavior. Partial success in accomplishing these objectives has been achieved during the course of this study.

Although not conclusively established as yet, there are strong indications that features contained in the OCPP data obtained in the "polarimetry" mode of operation at 0.935 microns contain information about the cloud formations below the high clouds previously studied in the ultraviolet at 0.365 microns. This conclusion is supported by the appearance and shapes of these features, their measured rotation rates, and very preliminary (and not well confirmed, as yet) correlation with NIR features. The procedures and programs for accomplishing correlations between OCPP and NIR data were completed during this study, but have only been applied in a very preliminary mode. Correlation of data sets requires appreciable labor to make the data sets compatible for analyses, and few such correlations were accomplished. However, using the analytical tools developed during the course of this study, examinations of more OCPP data sets and NIR correlations are in progress, under other auspices, and will be reported in the near future. The possible correlation of features in data sets taken with long time separations will also be studied to investigate the possible existence of long-lived processes in the Venus atmosphere.

In general 0.935 and 0.365 micron data sets taken nearly simultaneously have no apparent features common to both data sets. However, we have found that they do appear to have some rare common features, implying that they are viewing an overlapping altitude region at an altitude between those that characterize the major features seen in each data set. Although these common features are very difficult to distinguish in imagery created from the data sets, they are more easily apparent in the plots of data shown, for example in Figures 1a and 1b.

As part of this study new Earth-based NIR data was obtained for eight successive days in September, 1991, for attempts at correlation with PVO radio occultation data obtained during the same period. The NIR data were interesting in themselves, inasmuch as they confirmed the existence of long-lived opacity features in the cloud structure, features that had been previously seen in observations dating back several years. Unfortunately, the results derived from processing the four sets of pertinent occultation data obtained during this period, did not yield accurate absorptivities or sulfuric acid vapor concentrations in the regions immediately below the clouds. The cloud morphology, at some of the occultation site locations, was, also, not distinctive enough for differentiation with other occultation sites. It was, thus, not possible to associate the occultation-derived quantities with indicated NIR opacities in

the region of these occultation measurements, and no implications as to the constitution of the cloud particles in these regions may be drawn. However, excellent temperature profiles were obtained. These indicate that the higher temperature profile exists in a very differently processed portion of atmosphere than the lower temperature profiles. This result, as well as the indication of temperatures that vary in a mode characteristic of wave propagation through the atmosphere, gives strong implication of the existence of low wave number, and also much shorter wavelength, wave propagation in the atmosphere at these altitudes.

Again, under other auspices, using the improved analytical tools developed in the course of this study, we are investigating other PVO radio occultations taken during past seasons to see whether they may be processed to yield better absorptivity and sulfuric acid vapor profiles, especially for periods for which NIR data are available. In addition, we are looking into the possibility of correlation of the occultation data with available 0.935 micron PV OCPP data.

In conclusion, in this study we have begun to investigate the further use of PVO data for documenting Venus cloud and atmospheric properties and behavior. We have found promising features in the available data that may be used for these purposes, and have begun attempts to exploit them.

References

Allen, D. and J. W. Crawford, Nature, 307, 222 (1984).
Allen, D., D. Crisp and V. S. Meadows, Nature, October (1992)
Carlsen, R. W. et al., Science, 253, 1541 (1991).
Carlsen, R. W. et al., Planetary and Space Science, in press (1993).
Crisp, D. et al., Science, 246, 506 (1989).
Crisp, D., Bull. Amer. Astron. Soc., 22, 1053 (1990a).
Crisp, D., Trans. Amer. Geophys. Union, 71, 1430, (1990b).
Crisp, D. et al., Science, 253, 1263 (1991a).
Crisp, D. et al., Science, 253, 1538 (1991b).
Fahd, A. D. and P. G. Steffes, Icarus, 97, 200 (1992).
Fjeldbo, G. A., A. J. Kliore and V. R. Eshleman, Astron. J., 76, 123 (1971).
Hunten, D. L. et al., eds., Venus, The University of Arizona Press, Tucson, Arizona (1983).
Jenkins, J. M. and P. G. Steffes, Icarus, 90, 129 (1991).
Jenkins, J. M., Ph. D. Dissertation, Georgia Institute of Technology, (1992a).
Jenkins, J. M. and B. Ragent, Bull. Amer. Astron. Soc., 24, 1002 (1992b).
Kalas, P. and B. Ragent, Bull. Amer. Aston. Soc., 24, 997 (1992).
Kamp, L. W., F. W. Taylor and S. B. Calcutt, Nature, 336, 360 (1989).
Kamp, L. W. and F. W. Taylor, Icarus, 86, 510 (1990).
Kliore, A. J. and I. R. Patel, Icarus, 52, 320 (1982).
Knollenberg, R. G., Icarus, 57, 161 (1984).
Linkin, V. M. et al., Science, 231, 1420 (1986).
Limaye, S. S., Icarus, 57, 362 (1984).
McCaughean, M., Proceedings of the Third Infrared Detector Workshop, NASA TM 102209 (1989).
Mutch, T. A., ed., Pioneer Venus Special Issue, J. Geophys. Res., 85, 7573 et seq. (1980).
Ragent, B. et al., Advanc. Space Res., 5, 85 (1985).
Ragent, B. et al., Advanc. Space Res., 7, (1987)
Ragent, B. et al., Trans. Amer. Geophys. Union, 71, 1430 (1990).
Rossow, W. B., et al, J. Geophys. Res., 85, 8107 (1980).
Rossow, W. B., A. D. Del Genio and T. Eichler, J. Atm. Sciences, 47, 2053 (1990).
Schubert, G., in Venus (eds. Hunten, D. M. et al.), 681 (1983).
Seiff, A., in Venus (eds. Hunten, D. M. et al.), Appendix A, 1045 (1983).
Sinton, W. et al., Bull. Amer. Aston. Soc., 22, 1050 (1990).
Steffes, P. G., Icarus, 64, 576 (1985).
Steffes, P. G. et al., Bull. Amer. Astron. Soc., 23, 1196 (1991).
Toon, O. B. et al., Icarus, 57, 143 (1984).
Yee, S. M. T. and B. Ragent, in preparation.

Appendix A

Program to "Normalize" the OCPP Polarimetry Map by Removing the Gross Variation in the Intensity

(Program written by Larry Travis)

```
C*********************************************************************
C       THIS PROGRAM READS REFLECTION MATRICES, R(I,J), STORED IN A
C       DISK FILE (DSRN=10).  THESE MATRICES REPRESENT THE RESULTS OF
C       A MULTIPLE SCATTERING MODEL OF THE CLOUD-HAZE SYSTEM FOR VENUS
C       AND THUS ARE USED TO CALCULATE THE THEORETICAL RADIANCE FOR
C       ARBITRARY SCATTERING GEOMETRIES PRESCRIBED BY OBSERVER ZENITH
C       ANGLE (MU), SOLAR ZENITH ANGLE (MU0), AND DIFFERENCE IN THE
C       OBSERVER AND SOLAR AZIMUTHAL ANGLES (PMP0=PHI-PHI0).
C
C       THE MULTIPLE SCATTERING COMPUTATION REPRESENTS INTEGRATION
C       OVER ZENITH ANGLE SPACE BY GAUSSIAN QUADRATURE AND TREATS THE
C       AZIMUTHAL DEPENDENCE USING FOURIER SERIES DECOMPOSITION.  THUS,
C       THERE ARE REFLECTION MATRICES FOR EACH OF 30 FOURIER COMPONENTS
C       IN THIS SPECIFIC MODEL, AND EACH MATRIX IS COMPUTED AT THE 29
C       GAUSSIAN QUADRATURE VALUES OF MU/MU0 (SPECIFIC MU/MU0 VALUES
C       ARE REGENERATED HERE WITH THE CALL TO SUBROUTINE GAUSST).
C
C       THIS PROGRAM THUS READS IN THE MATRICES, RESCALES THEM USING
C       FUNCTIONAL DEPENDENCIES OF MU AND MU0 TO ENHANCE ACCURACY OF
C       INTERPOLATION, READS IN THE OBSERVED POLARIMETRY MAP INTENSITY
C       DATA TAGGED WITH SCATTERING GEOMETRY, AND INTERPOLATES THE
C       REFLECTION MATRICES AND PERFORMS THE FOURIER SUMS FOR THE
C       OBSERVATION SCATTERING GEOMETRIES TO DETERMINE THE APPROPRIATE
C       THEORETICAL INTENSITY (TINT(ELMENT,ROW)) TO "NORMALIZE" THE
C       POLARIMETRY MAP BY REMOVING THE GROSS GEOMETRIC VARIATION IN
C       THE INTENSITY.
C*********************************************************************
      IMPLICIT REAL*8 (A-H,O-Z)
      COMMON XMU(30),WEIGHT(30)
      COMMON /RMBLK/ RM(30,30,30)
      REAL*8 MU,MU0
      REAL*4 R(30,30),OINT(120,72),TINT(120,72),PHS(120,72)
      CHARACTER*1 CARD(80),CARDE(80),HDREC(2880)
      INTEGER*4 IINT(120,72),IPOL(120,72),IPDIR(120,72),ITIME(120,72),
     *ILAT(120,72),ILON(120,72),IOZEN(120,72),ISZEN(120,72),
     *IPMP0(120,72),IDATA(720,108),NINT(120,72),HIST(2000)
      EQUIVALENCE (IDATA(1,1),IINT(1,1)),(IDATA(1,13),IPOL(1,1)),
     *(IDATA(1,25),IPDIR(1,1)),(IDATA(1,37),ITIME(1,1)),
     *(IDATA(1,49),ILAT(1,1)),(IDATA(1,61),ILON(1,1)),
     *(IDATA(1,73),IOZEN(1,1)),(IDATA(1,85),ISZEN(1,1)),
     *(IDATA(1,97),IPMP0(1,1))
      PI=3.141592653589793D0
      RADCON=PI/180.D0
      NTH=29
C*********************************************************************
C       GENERATE THE SET OF MU/MU0 VALUES FOR WHICH THE
C       REFLECTION MATRICES WERE COMPUTED.  THESE ARE OBTAINED
C       USING SUBROUTINE GAUSST, WITH THE MU VALUES STORED IN
C       ARRAY, XMU.
      CALL GAUSST(NTH,0.D0,1.D0,XMU,WEIGHT)
C*********************************************************************
C*********************************************************************
C       READ IN THE REFLECTION MATRIX, R(I,J), FOR FOURIER COMPONENT
C       NUMBER 1, RESCALE THE MATRIX BY MULTIPLYING BY MU+MU0+1.0D-10,
C       AND STORE IN MATRIX RM, WHICH IS SUPPLIED TO THE INTERPOLATION
C       SUBROUTINE INTERP THROUGH THE COMMON BLOCK RMBLK.
C       THE FILE CONTAINING THE REFLECTION MATRICES IS IN CARD IMAGE
C       FORMAT, WITH 5 ELEMENTS PER CARD: 5E15.7
      DO 100 J=1,30
100   READ(10,8001) (R(I,J),I=1,30)
8001  FORMAT(5E15.7)
      DO 110 J=1,NTH
      XMUJ=XMU(J)
      DO 110 I=1,NTH
110   RM(I,J,1)=(XMU(I)+XMUJ+1.D-10)*R(I,J)
C*********************************************************************
```

```
C*************************************************************************
C       READ IN THE REFLECTION MATRIX, R(I,J), FOR FOURIER COMPONENTS
C       2 THROUGH 30, RESCALE THE MATRICES, AND STORE IN MATRIX RM.
C       THE INVERSE OF THE RESCALING IS APPLIED IN SUBROUTINE INTERP
C       AFTER THE INTERPOLATION IN MU AND MU0.
      DO 130 M=2,30
      DO 115 J=1,30
115   READ(10,8001) (R(I,J),I=1,30)
      DO 120 J=1,NTH
      XMUJ=XMU(J)
      XMUJS=XMUJ*XMUJ
      DO 120 I=1,NTH
      XMUI=XMU(I)
120   RM(I,J,M)=(XMUI+XMUJ+1.D-10)*R(I,J)/DSQRT((1.D0-XMUJS
     *+1.D-10)*(1.D0-XMUI*XMUI+1.D-10))
130   CONTINUE
C*************************************************************************
C*************************************************************************
C       READ IN THE FIRST BLOCK OF THE FITS FORMAT POLARIMETRY DATA FILE,
C       NAMELY, THE FITS HEADER RECORD CONSISTING OF 36 CARD IMAGES.
C       THE CHARACTER VARIABLE, HDREC, IS USED HERE TO INPUT THE BLOCK,
C       AND THEN EACH OF THE 36 CARD IMAGES IS PLACED IN TURN IN THE
C       VARIABLE, CARD.  SINCE THE FITS HEADER RECORD IS IN ASCII FORMAT,
C       THE VARIABLE, CARD, IS THEN CONVERTED TO EBCDIC FORMAT IN THE
C       CORRESPONDING VARIABLE, CARDE, USING OUR GISS FACILITY FUNCTION,
C       EBCDIC.  REMOVE OR REPLACE THIS CONVERSION STATEMENT FOR
C       APPLICATION AT A DIFFERENT FACILITY.
      READ(20,8002) HDREC
8002  FORMAT(36(80A1))
      DO 200 NCD=1,36
      DO 190 M=1,80
190   CARD(M)=HDREC(80*(NCD-1)+M)
      CALL EBCDIC(CARD,80,CARDE)
200   WRITE(6,9001) CARDE
9001  FORMAT(1H ,80A1)
C*************************************************************************
C*************************************************************************
C       READ IN THE POLARIMETRY MAP DATA FROM THE FITS FORMAT FILE.
C       HERE WE INPUT ONLY THE 108 RECORDS FOLLOWING THE HEADER RECORD
C       JUST READ IN; THESE CORRESPOND TO THE DATA FOR THE 935 NM BAND
C       ONLY.  DATA FOR THE 550, 365, AND 270 NM BANDS FOLLOW IN THE
C       REMAINING 324 RECORDS IN THE FILE.  THE 935 NM DATA IS READ IN
C       TO THE VARIABLE, IDATA(720,108), WHICH IS EQUIVALENCED TO THE
C       120 BY 72 ARRAYS: IINT - INTENSITY, IPOL - POLARIZATION DEGREE,
C       IPDIR - POLARIZATION DIRECTION, ITIME - TIME, ILAT - LATITUDE,
C       ILON - LONGITUDE, IOZEN - OBSERVER ZENITH ANGLE, ISZEN - SOLAR
C       ZENITH ANGLE, IPMP0 - DIFFERENCE IN AZIMUTHAL ANGLES.
      DO 210 NREC=1,108
210   READ(20,8003) (IDATA(K,NREC),K=1,720)
8003  FORMAT(20(36A4))
      DO 220 N=1,72
      DO 220 J=1,120
      PHS(J,N)=0.0
      OINT(J,N)=IINT(J,N)
      TINT(J,N)=0.0
220   NINT(J,N)=0
      NCNT=0
      OISUM=0.D0
      TISUM=0.D0
C*************************************************************************
C       THE FOLLOWING LOOP FINDS THE SUMS OF THE OBSERVED INTENSITIES
C       (OISUM) AND THEORETICAL INTENSITIES (TISUM) FOR ALL POLARIMETRY
C       MAP ELEMENTS ON THE DISK (MU AND MU0 GREATER THAN 0).  THE RATIO
C       OF THOSE SUMS, FACTI=OISUM/TISUM, IS THEN USED TO SCALE THE
C       THEORETICAL INTENSITIES.  THUS, THE DIFFERENCES BETWEEN OBSERVED
C       AND SCALED THEORETICAL INTENSITIES THEN CLUSTER ABOUT 0 DN.
```

```
      DO 310 N=1,72
      DO 310 J=1,120
      IF(IOZEN(J,N).LT.0.D0) GO TO 300
      MU=DCOS(IOZEN(J,N)*RADCON/10.0)
      MU0=DCOS(ISZEN(J,N)*RADCON/10.0)
      PMP0=IPMP0(J,N)*RADCON/10.0
      IF(MU.LE.0.D0.OR.MU0.LE.0.D0) GO TO 300
      IF(OINT(J,N).LE.0.0) GO TO 300
      CALL INTERP(MU,MU0,PMP0,NTH,30,SI)
      CPHS=MU0*MU-DSQRT((1.D0-MU**2)*(1.D0-MU0**2))*DCOS(PMP0)
      PHASE=DARCOS(CPHS)/RADCON
      NCNT=NCNT+1
      OISUM=OISUM+OINT(J,N)
      TISUM=TISUM+SI
      PHS(J,N)=PHASE
      TINT(J,N)=SI
300   CONTINUE
310   CONTINUE
      FACTI=OISUM/TISUM
C*****************************************************************************
      WRITE(6,9002) NCNT,OISUM,TISUM,FACTI
9002  FORMAT(1H1,' NUMBER OF MAP ELEMENTS ON THE DISK (MU AND MU0',
     *' GREATER THAN 0.0):',I6,//,1X,' SUM OF OBSERVED INTENSITIES:',
     *F11.1,//,1X,' SUM OF THEORETICAL INTENSITIES:',F9.3,//,1X,
     *' FACTOR FOR SCALING THEORETICAL INTENSITIES:',F10.3)
      DO 600 N=1,72
      WRITE(6,9003)
9003  FORMAT(1H1,'INT(OBS)  INT(TH)    DEL      LAT       LON      MU',
     *8X,'MU0        PMP0     PHASE',/)
      DO 600 J=1,120
      OBI=OINT(J,N)
      SI=TINT(J,N)
      PHASE=PHS(J,N)
      DEL=0.0
      MU=-1.0
      MU0=0.0
      PMP0=0.0
      IF(IOZEN(J,N).LT.0.D0) GO TO 590
      MU=DCOS(IOZEN(J,N)*RADCON/10.0)
      MU0=DCOS(ISZEN(J,N)*RADCON/10.0)
      PMP0=IPMP0(J,N)/10.0
      IF(MU.LE.0.D0.OR.MU0.LE.0.D0) GO TO 590
      IF(SI.LE.0.0.OR.OBI.LE.0.0) GO TO 590
C*****************************************************************************
C       THE VARIABLE, DEL, REPRESENTS THE NORMALIZED DIFFERENCE OF THE
C       OBSERVED AND SCALED THEORETICAL INTENSITIES, EXPRESSED IN TENTHS
C       OF A PERCENT AND WITH AN ADDITIVE CONSTANT OF 128 TO KEEP MOST
C       OF THE NUMBERS POSITIVE.  THE INDIVIDUAL DEL VALUES ARE SAVED
C       IN ARRAY, NINT, FOR OUTPUT OR FURTHER PROCESSING.
      DEL=2000.0*(OBI-FACTI*SI)/(OBI+FACTI*SI)+128.0
      IF(DEL.LT.0.D0) DEL=0.D0
      NINT(J,N)=DEL
590   CONTINUE
      ALAT=ILAT(J,N)/10.0
      ALON=ILON(J,N)/10.0
600   WRITE(6,9004) OBI,SI,DEL,ALAT,ALON,MU,MU0,PMP0,PHASE
9004  FORMAT(1H ,F7.1,F10.5,F7.1,2F10.2,2F10.4,2F10.2)
      DO 700 I=1,2000
700   HIST(I)=0
      DO 750 N=1,72
      DO 750 J=1,120
      IWV=NINT(J,N)
      IF(IWV.GT.500) GO TO 710
      HIST(1+IWV)=HIST(1+IWV)+1
      GO TO 740
710   HIST(501)=HIST(501)+1
```

```
740   CONTINUE
750   CONTINUE
      WRITE(6,9005)
9005  FORMAT(1H1,' HISTOGRAM OF INTENSITY VALUES',/)
      WRITE(6,9006) (I-1,HIST(I),I=1,501)
9006  FORMAT(10(1X,I7,I5))
      STOP
      END
      SUBROUTINE INTERP(MU,MU0,PMP0,NTH,MCAP,SI)
      IMPLICIT REAL*8 (A-H,O-Z)
      COMMON XMU(30),WEIGHT(30)
      COMMON /RMBLK/ RM(30,30,30)
      REAL*8 MU,MU0,INTENS,DMU(29)
      DATA INIT/0/
      IF(INIT.NE.0) GO TO 110
      INIT=1
      NTHM1=NTH-1
      DO 100 I=1,NTHM1
100   DMU(I)=XMU(I+1)-XMU(I)
110   CONTINUE
      DO 120 I=2,NTH
      IF(MU.LT.XMU(I)) GO TO 130
120   CONTINUE
      II=NTH
      GO TO 135
130   II=I
135   CONTINUE
      DO 140 J=2,NTH
      IF(MU0.LT.XMU(J)) GO TO 150
140   CONTINUE
      JJ=NTH
      GO TO 155
150   JJ=J
155   CONTINUE
      IF(II.EQ.2) GO TO 160
      IF(II.EQ.NTH) GO TO 170
      IIM2=II-2
      IIM1=II-1
      IIP1=II+1
      D1=DMU(IIM2)
      D2=DMU(IIM1)
      D3=DMU(II)
      XX1=MU-XMU(IIM2)
      XX2=MU-XMU(IIM1)
      XX3=MU-XMU(II)
      XX4=MU-XMU(IIP1)
      A1=-XX2*XX3*XX3/(D2*D1*(D2+D1))
      A2=XX1*XX3*XX3/(D2*D2*D1)+XX2*XX3*XX4/(D2*D2*(D2+D3))
      A3=-XX1*XX2*XX3/(D2*D2*(D2+D1))-XX2*XX2*XX4/(D2*D2*D3)
      A4=XX2*XX2*XX3/(D2*D3*(D2+D3))
      GO TO 180
160   IIM2=1
      IIM1=1
      IIP1=3
      D1=DMU(1)
      D2=DMU(2)
      XX1=MU-XMU(1)
      XX2=MU-XMU(2)
      XX3=MU-XMU(3)
      A1=0.D0
      A2=XX2*XX3/(D1*(D2+D1))
      A3=-XX1*XX3/(D1*D2)
      A4=XX1*XX2/(D2*(D2+D1))
      GO TO 180
170   IIM2=NTH-2
      IIM1=NTHM1
```

```
      IIP1=NTH
      D1=DMU(IIM2)
      D2=DMU(IIM1)
      XX1=MU-XMU(IIM2)
      XX2=MU-XMU(IIM1)
      XX3=MU-XMU(II)
      A1=XX2*XX3/(D1*(D1+D2))
      A2=-XX1*XX3/(D1*D2)
      A3=XX1*XX2/(D2*(D1+D2))
      A4=0.D0
180   CONTINUE
      IF(JJ.EQ.2) GO TO 190
      IF(JJ.EQ.NTH) GO TO 200
      JJM2=JJ-2
      JJM1=JJ-1
      JJP1=JJ+1
      D1=DMU(JJM2)
      D2=DMU(JJM1)
      D3=DMU(JJ)
      YY1=MU0-XMU(JJM2)
      YY2=MU0-XMU(JJM1)
      YY3=MU0-XMU(JJ)
      YY4=MU0-XMU(JJP1)
      B1=-YY2*YY3*YY3/(D2*D1*(D2+D1))
      B2=YY1*YY3*YY3/(D2*D2*D1)+YY2*YY3*YY4/(D2*D2*(D2+D3))
      B3=-YY1*YY2*YY3/(D2*D2*(D2+D1))-YY2*YY2*YY4/(D2*D2*D3)
      B4=YY2*YY2*YY3/(D2*D3*(D2+D3))
      GO TO 210
190   JJM2=1
      JJM1=1
      JJP1=3
      D1=DMU(1)
      D2=DMU(2)
      YY1=MU0-XMU(1)
      YY2=MU0-XMU(2)
      YY3=MU0-XMU(3)
      B1=0.D0
      B2=YY2*YY3/(D1*(D1+D2))
      B3=-YY1*YY3/(D1*D2)
      B4=YY1*YY2/(D2*(D1+D2))
      GO TO 210
200   JJM2=NTH-2
      JJM1=NTHM1
      JJP1=NTH
      D1=DMU(JJM2)
      D2=DMU(JJM1)
      YY1=MU0-XMU(JJM2)
      YY2=MU0-XMU(JJM1)
      YY3=MU0-XMU(JJ)
      B1=YY2*YY3/(D1*(D1+D2))
      B2=-YY1*YY3/(D1*D2)
      B3=YY1*YY2/(D2*(D1+D2))
      B4=0.D0
210   CONTINUE
      SFACT=DSQRT((1.D0-MU*MU+1.D-10)*(1.D0-MU0*MU0+1.D-10))
      FSUM=0.D0
      DO 300 M=1,MCAP
      CPMP0=DCOS((M-1.D0)*PMP0)
      F11=RM(IIM2,JJM2,M)
      F21=RM(IIM1,JJM2,M)
      F31=RM(II,JJM2,M)
      F41=RM(IIP1,JJM2,M)
      F12=RM(IIM2,JJM1,M)
      F22=RM(IIM1,JJM1,M)
      F32=RM(II,JJM1,M)
      F42=RM(IIP1,JJM1,M)
```

```
      F13=RM(IIM2,JJ,M)
      F23=RM(IIM1,JJ,M)
      F33=RM(II,JJ,M)
      F43=RM(IIP1,JJ,M)
      F14=RM(IIM2,JJP1,M)
      F24=RM(IIM1,JJP1,M)
      F34=RM(II,JJP1,M)
      F44=RM(IIP1,JJP1,M)
      F1=A1*F11+A2*F21+A3*F31+A4*F41
      F2=A1*F12+A2*F22+A3*F32+A4*F42
      F3=A1*F13+A2*F23+A3*F33+A4*F43
      F4=A1*F14+A2*F24+A3*F34+A4*F44
      F=B1*F1+B2*F2+B3*F3+B4*F4
      IF(M.EQ.1) GO TO 280
      F=2.0*F*SFACT
280   CONTINUE
      FSUM=FSUM+F*CPMP0
300   CONTINUE
      SI=FSUM*MU0/(MU+MU0+1.D-10)
      RETURN
      END
      SUBROUTINE GAUSST(N,XL,XU,SS,TT)
      IMPLICIT REAL*8(A-H,O-Z)
      DIMENSION Z(500),PA(500),W(500),R(500),SS(1),TT(1)
      TOL = 1.0D-16
      PI = 3.141592653589793D+00
      AA = 2.0D+00/PI**2
      AB = -62.0D+00/(3.0D+00*PI**4)
      AC = 15116.0D+00/(15.0D+00*PI**6)
      AD = -12554474.D+00/(105.0D+00*PI**8)
      PA(1) = 1.D0
      EN = N
      NP1 = N+1
      U = 1.0D+00-(2.0D+00/PI)**2
      D = 1.0D+00/DSQRT((EN+0.5D+00)**2+U/4.0D+00)
      DO 100  I = 1,N
      SM = I
      AZ = 4.0D+00*SM-1.0D+00
      AE = AA/AZ
      AF = AB/AZ**3
      AG = AC/AZ**5
      AH = AD/AZ**7
  100 Z(I) = 0.25D+00*PI*(AZ+AE+AF+AG+AH)
      DO 200  K = 1,N
      X = DCOS(Z(K)*D)
    1 PA(2) = X
      DO 201  NN = 3,NP1
      ENN = NN-1
  201 PA(NN) = ((2.0D+00*ENN-1.0D+00)*X*PA(NN-1)-(ENN-1.0D+00)*PA(NN-2))
     +         /ENN
      PNP = EN*(PA(N)-X*PA(NP1))/(1.0D+00-X*X)
      XI = X-PA(NP1)/PNP
      XD = DABS(XI-X)
      XDD = XD-TOL
      IF (XDD) 3,3,2
    2 X = XI
      GO TO 1
    3 R(K) = X
  200 W(K) = 2.0D+00*(1.0D+00-X*X)/(EN*PA(N))**2
      AP = (XU-XL)/2.D0
      BP = (XU+XL)/2.D0
      DO 300  I = 1,N
      M=N-I+1
      SS(M)=BP+AP*R(I)
300   TT(M)=AP*W(I)
      RETURN
```

Appendix B

Program to Identify Features Occurring in Two Images by Establishing the Existence of Relationships within Prescribed Limits, Identifying the Latitude-Longitude Coordinates of these Features in the Two Images, and Calculating Their Rotation Rate and Zonal Velocity

(Program written by David Crisp)

Figure Captions

Figure 1a. Plot of ln ($I\mu$) versus ln ($\mu\mu_o$), 365 nm data of the PV OCPP polarimetry mode image 4053 obtained on February 16,1990. The straight line is a least squares fit used to determine the constants to be used in the Minnaert function. The features marked with arrows are to be compared with those noted in Figure 1b.

Figure 1b. Same type of plot as that of Figure 1a, except for 935 nm data taken nearly simultaneously as those plotted in Figure 1a. The features noted by arrows are to be compared with those similarly marked in Figure 1a.

Figure 1c. Truncated Minnaert method plot similar to Figure 1a except that the data plotted and used for the straight line fit, have been limited to values for ln ($\mu\mu_o$) > -2.5.

Figure 1d. Plot similar to Figure 1b except that the data plotted and used for the straight line fit, have been limited to values for ln ($\mu\mu_o$) > -2.5.

Figure 2a. Image of 935 nm radiation from the bright side of Venus obtained by the Pioneer Orbiter OCPP experiment, operating in its "polarimetry" mode, on February 10, 1990. The image has been process using a specially developed multiple-scattering limb-darkening correction algorithm developed by Co-Investigator L. Travis to remove the gross intensity (see Appendix A). Much detailed structure, presumably attributable to cloud patterns, is evident in the image.

Figure 2b. Image of the same 935 nm data as those processed and shown in Figure 2a, but here processed using a stretched, truncated, Minnaert approach discussed in the text. Many common features are apparent in the two images.

Figure 2c. Image of 365 nm data taken nearly simultaneously with the 935 nm data shon in processed form in Figures 2a and 2b. The apparent features are strikingly different in the images derived from the two sets of data.

Figure 3a. Mosaic of images made from processed 935 nm data obtained by the Pioneer Venus Orbiter Cloud Photo-Polarimeter experiment on February 15, 16, 18, and 19, 1990 (images 4052, 4053, 4054, and 4055), in its

polarimetry mode of operation. The data are shown on a latitude-longitude projection, made assuming a 6 day feature rotation period. These data have been processed using a truncated Minnaert function, and the resulting intensities were power-law "stretched" before being presented.

Figure 3b. Similar to Figure 3a, but with intensities reversed to accentuate features.

Figure 3c. Similar to Figure 3a, but for an assumed zonal rotation period of 10 days.

Figure 4. A collection of Earth-based near infrared images of the dark side of Venus from a concerted effort to document the spatial distribution of infrared emissions. The 1.74 micron images in the top row and the first two in the second row, reading from left to right, were obtained at the Kitt Peak National Observatory, on 12/31/89, 1/1/90, 1/2/90, 1/4/90, 1/5/90, 1/6/90, and 1/7/90. The next three images in the second row from the top, and the first three images in the third row were obtained using a 2.36 micron filter at telescopes on Mauna Kea, Hawaii on 1/29/90, 1/31/90, 2/5/90, 2/7/90, 2/9/90, and 2/10/90. The last two images in row three were taken using a 2.42 micron filter with the 200" telescope on Mt. Palomar on 2/11/90 and 2/12/90. The last three images were obtained with a 2.36 micron filter at the Anglo-Australian Observatory at Siding Wells, Australia on 2/13/90, 2/14/90 and 2/15/90.

Figure 5a. Images of Venus night side data shown in Figure 4 projected onto a cylindrical latitude-longitude grid and then assembled into a mosaic for data extending from 12/31/89 to January 7, 1990 assuming a 5.5 day rotation period for image longitude registration and all longitude offsets referenced to 00:00 UT on February 10, 1990 (Crisp et al., 1991b).

Figure 5b. Same as for Figure 5a, except for images taken ooon February 7, 1990 to February 15, 1990. The alignment of the images to form the mosaics verifies the validity of the 5.5 day rotation period for many features, and the similarity of the large scale features in the two mosaics shows that the largest features endure for over a month. The small scale features apparently often persist for more than one rotation period (Crisp et al., 1991b).

Figure 6. Plot of feature velocities as a function of latitude. All tracking results from the January and February, 1990 programs were combined to derive these near-infrared feature velocities as a function of

latitude. The error bars show one standard deviation uncertainties in each five degree bin. The largest and smallest features have different velocity distributions at low latitudes. In general the large-scale features move faster than the small-scale features (Crisp et al., 1991b).

Figure 7. Preliminarily processed images of Venus each taken at about 1430 UT each day , using University of Hawaii Institute for Astronomy 24" telescope on Mauna Kea Hawaii, a NICMOS HgCdTe infrared camera with a 256x256 detector array and a filter centered at 2.35 microns. The images were taken, top row, left to right on September 14, 15, 16, 17 and 18, 1991, and, middle row, left to right, on September 19, 20, and 21, 1991. The two images in the bottom row were taken on September 28 and 30, 1991 with the UH 2.2 m telescope, and have not been corrected for scattered light from the bright crescent.

Figure 8. Mosaic of images taken during (a) June 24-28, 1988 (top mosaic) using the University of Hawaii Institute for Astronomy 2.2 m telescope on Mauna Kea, an infrared camera with a 128x128 detector array with a band pass filter centered on 2.35 microns, and, (b) September 14-21, 1991 (bottom mosaic) with the 24" telescope of the University of Hawaii Institute for Astronomy on Mauna Kea, Hawaii, using an infrared camera and a 256x256 detector array with a band pass filter centered at 2.35 microns. An atmospheric rotation period of 5.5 days has been assumed. Considerable processing of the original images has been done, including flatfielding, background subtraction, removal of scattered light, coadding of multiple images, geometric rectification, projection onto a latitude-longitude grid, and adjustment of range of intensities to produce better cross image matching ("rubber-sheeting" adjustment of both sides of a projected image is yet to be accomplished). All of the images in the bottom mosaic have been referenced to the sub-earth point latitude-longitude coordinates of the center of the image obtained on September 17, 1991.

Figure 9a. Mosaics for the September, 1991 data, similar to the mosaic shown in Figure 8, but for assumed atmospheric rotation periods of, top to bottom, 4, 5, 6, and 7 days.

Figure 9b. (1) Similar to the mosaics for the September, 1991 data shown in Figure 9a but with a latitude-longitude grid superposed. The time for the image obtained on September 14, 1991 (15:00 UT) was used as the mosaic reference. An assumed atmospheric rotation period of

5.5 days was used, and the derived locations of several radio occultation measurements have been indicated (see text). (2) Same as (1) with intensities reversed.

Figure 9c. Similar to Figure 9b, except for an assumed atmospheric rotation period of 4 days.

Figure 9d. Similar to Figure 9b, except for an assumed atmospheric rotation period of 5 days.

Figure 9e. Similar to Figure 9b, except for an assumed atmospheric rotation period of 6 days.

Figure 9f. Similar to Figure 9b, except for an assumed atmospheric rotation period of 7 days.

Figure 9g. Similar to Figure 9b, except for an assumed atmospheric rotation period of 8 days.

Figure 9h. Similar to Figure 9b, except for an assumed atmospheric rotation period of 10 days.

Figure 10. Plot of the value of the standard deviation of the derived atmospheric temperature plotted against radius (Venus radius assumed to be 6052 km) for the PV radio occultation data of orbit 4661 on September 10, 1991.

Figure 11a. Plots of the derived profiles of atmospheric temperature as a function of altitude above the assumed planetary radius of 6052 km for PV orbits 4661, 4663, 4668, and 4670, corresponding to 1991 September 10, 12, 17, and 19, respectively.

Figure 11b. Expanded plots of temperature-altitude profiles derived for orbits 4661, 4663 and 4670 (1991 September 10, 12 and 19).

Figure 11c. Altitude plots of derived 13 cm absorptivities for the occultations obtained for PV orbits 4661, 4663, 4668 and 4670. Unfortunately, although not shown on these plots, the errors estimated in the derived absorptivities are so large that no conclusions as to the actual behavior of absorptivity with altitude should be drawn from these plots (see text).

Figure 12a. Plot of derived atmospheric temperatures versus pressure for occultations for PV orbits 4661,4663 and 4670. A reference curve of temperature versus pressure (Seiff, 1983) is plotted for comparison.

Figure 12b. Plots of temperature versus pressure measured by the two balloons of the Vega Mission (Linkin et al.,

1986).

Figure 13. Altitude plots of differences between derived atmospheric densities and a reference density profile (Seiff, 1983). The difference for the data derived from the occultation of orbit 4670 is strikingly different from the differences derived for orbits 4661 and 4663.

Figure 14a. Altitude plots of the temperature residuals for the temperatures plotted in Figure 11a after essentially high pass filtering to emphasize the rapid variations in temperature with altitude. The cases shown are for filtering with a 10 km cutoff high pass filter. Each plot is displaced from the zero temperature coordinate for clarity of presentation, and has lines superposed showing one standard deviation.

Figure 14b. Altitude plots of temperature residuals for PV orbit 4661 (September 10, 1991) showing the effects of using filters cutoff at 5, 10 and 11 km.

Fifure 14c. Altitude plots of temperature residuals obtained by using an essentially very low cutoff frequency filter. The slower variations of the temperature with altitude is more evident in this plot as compared with those in Figure 14a.

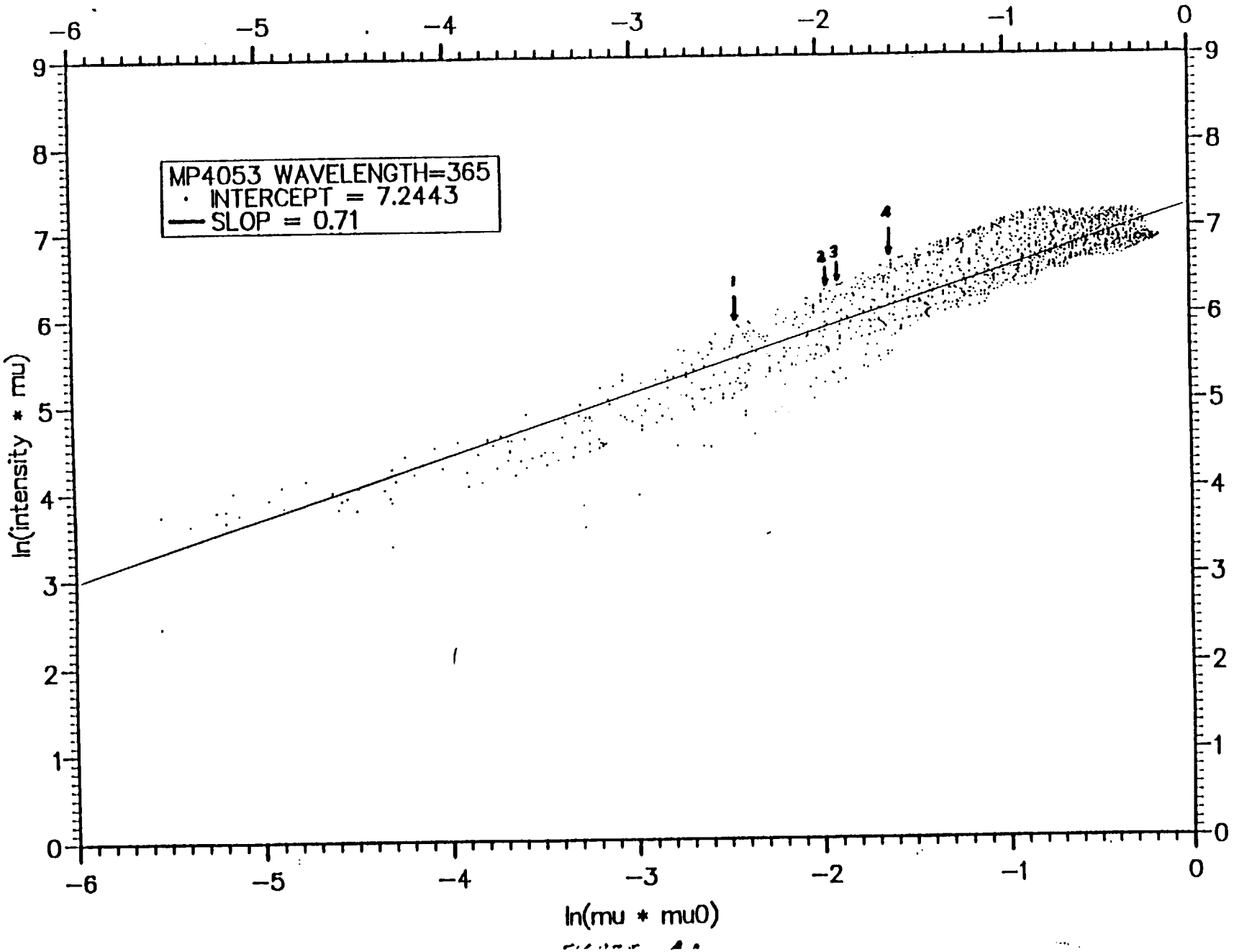
MP4053 WAVELENGTH=365
INTERCEPT = 7.2443
SLOP = 0.71
ln(intensity * mu)
ln(mu * mu0)
-6
-5
-4
-3
-2
-1
0
1
2
3
4
5
6
7
8
9

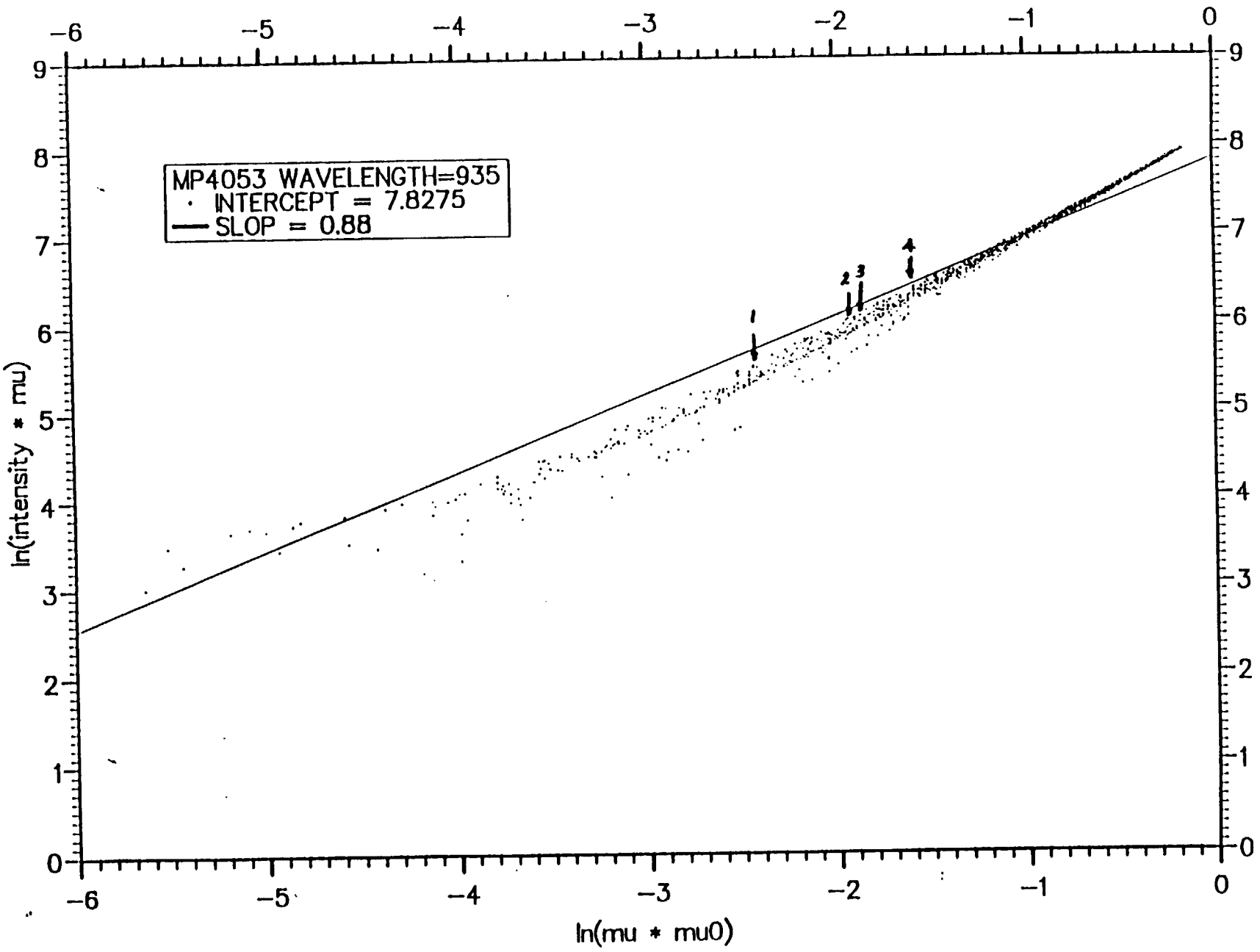
MP4053 WAVELENGTH=935
INTERCEPT = 7.8275
SLOP = 0.88
ln(intensity * mu)
ln(mu * mu0)
1
2
3
4

FIGURE 16

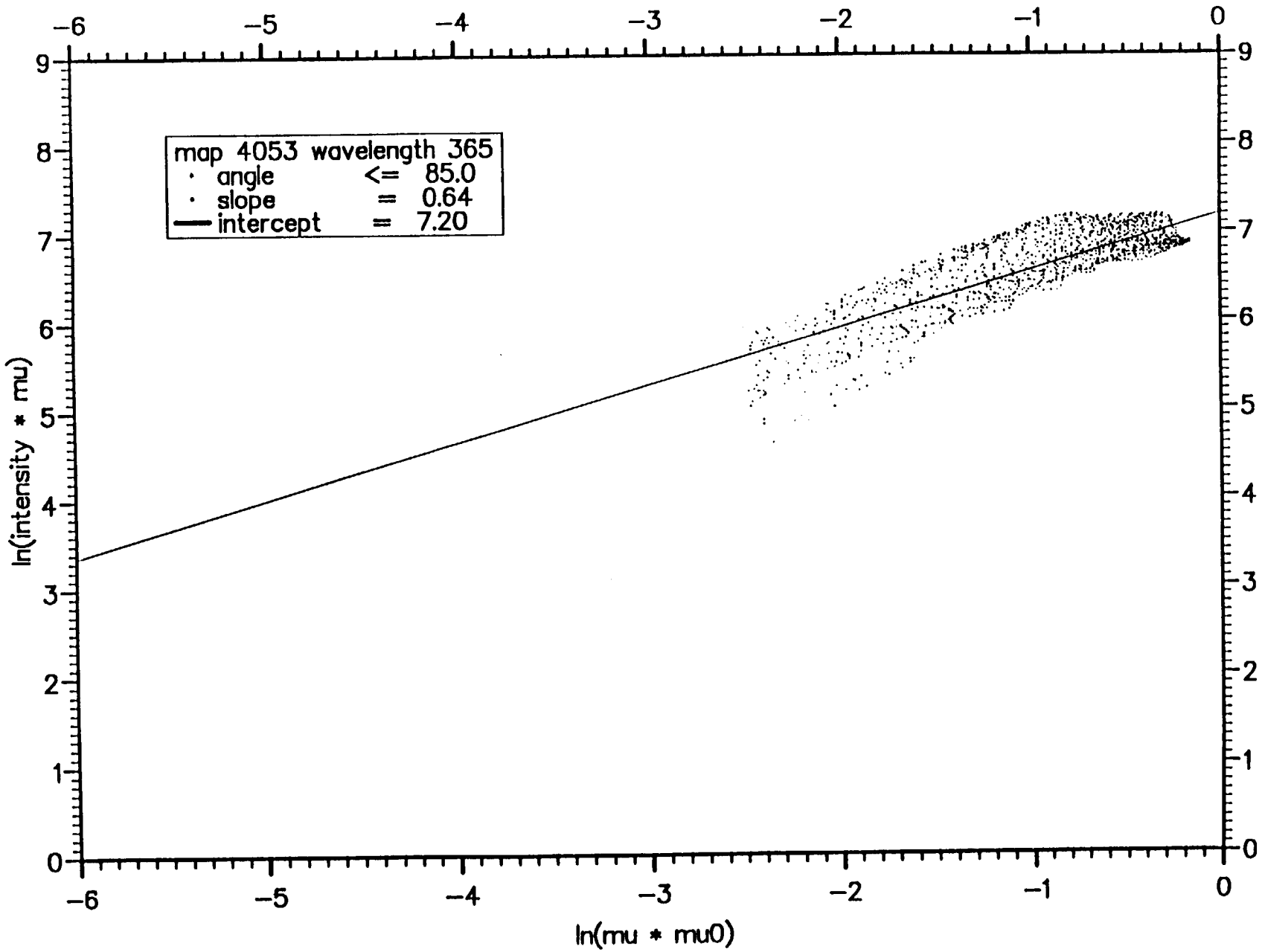
map 4053 wavelength 365
· angle <= 85.0
· slope = 0.64
— intercept = 7.20
ln(intensity * mu)
ln(mu * mu0)
-6
-5
-4
-3
-2
-1
0
1
2
3
4
5
6
7
8
9

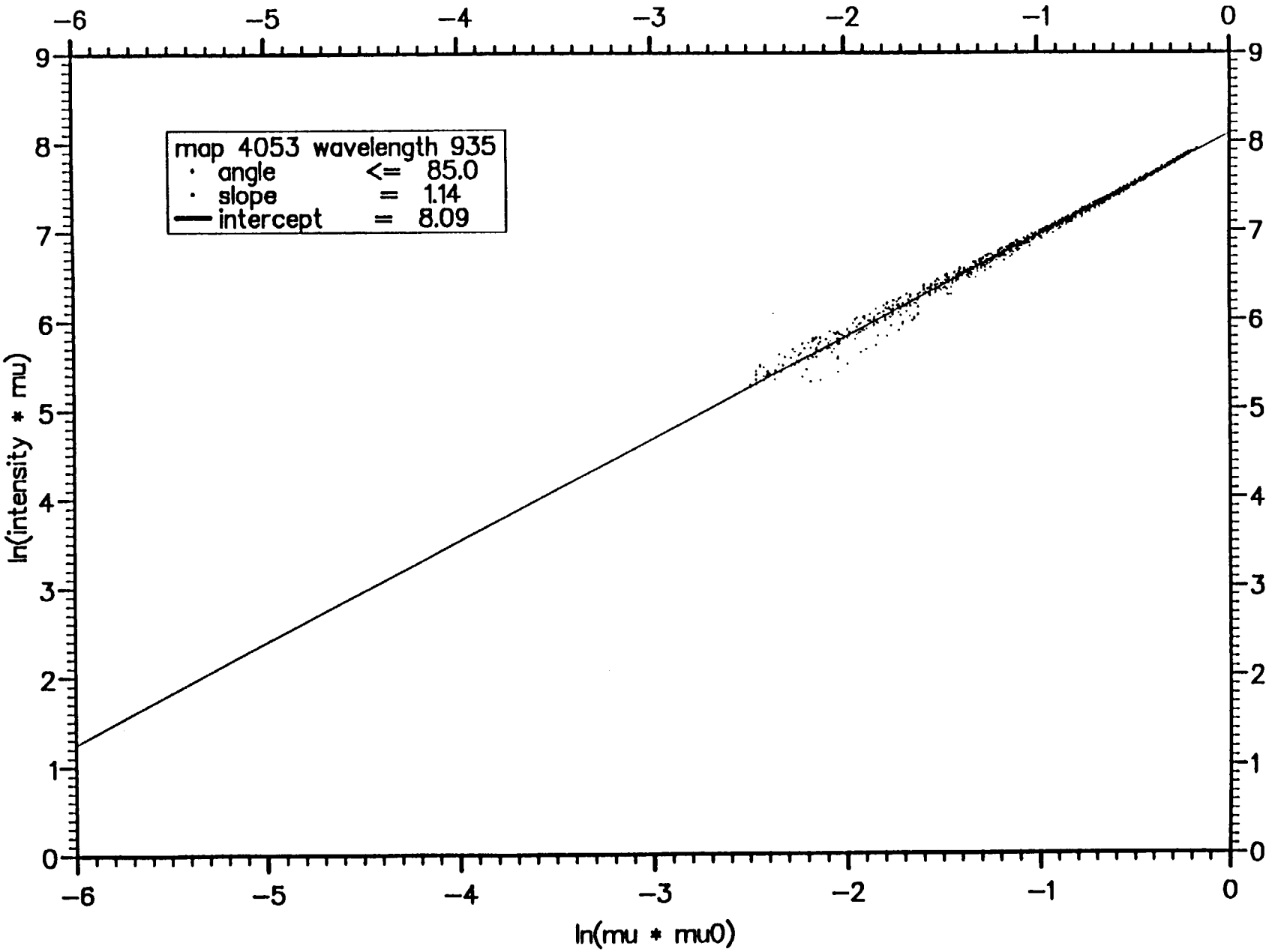
map 4053 wavelength 935
angle <= 85.0
slope = 1.14
intercept = 8.09
ln(intensity * mu)
ln(mu * mu0)
-6
-5
-4
-3
-2
-1
0
9
8
7
6
5
4
3
2
1
0

Figure 1d

```
.....................................................
      program winds
c
ccccccccccccccccccccccccccccc  w i n d s  ccccccccccccccccccccccccccccc
cc                                                                    cc
cc                                                                    cc
cc    p u r p o s e :                                                 cc
cc                                                                    cc
cc    this program reads lat-lon maps of a planet, obtained at        cc
cc    different times, and finds the feature rotation rate by shifting cc
cc    the maps in longitude, finding the rms and absolute difference  cc
cc    between the maps at each position.  it defines the longitude    cc
cc    shift that gives the smallest rms or absolute difference in     cc
cc    each longitude bin is chosen as the best fit.  it then finds    cc
cc    the rotation rate and zonal velocity corresponding to that     .cc
cc    shift.                                                          cc
cc                                                                    cc
cc    note:   if the rotation is retrograde, the value for the initial cc
cc            period must be negative.                                cc
cc                                                                    cc
cc                                                                    cc
cc    i n p u t :                                                     cc
cc                                                                    cc
cc      radkm - distance from center of planet of layer being tracked, cc
cc              (km), ie radkm = radius of planet + altitude of layer cc
cc    fileout - name of output file with feature-tracking results.    cc
cc       wlon - longitude range of lat-lon patch (degrees)            cc
cc       wlat - latitude range of lat-lon patch (degrees)             cc
cc       perd - nominial period of rotation of layer (days)           cc
cc      nlon0 - number of pixels to be scanned in longitude to find   cc
cc              best alignment of two images for given lat-lon box.   cc
cc      nlon0 - number of pixels to be scanned in latitude to find    cc
cc              best alignment of two images for given lat-lon box.   cc
cc    overlap - minimum fraction of the number of pixels in two boxes cc
cc              that must overlap for a valid wind speed estimate.    cc
cc     varmin - mininum fraction of variance in reference box that    cc
cc              must beaccounted for at position of best alignment.   cc
cc    rmxbxmm - minimum fractional rms within a box to establish that cc
cc              it includes one or more features.                     cc
cc     errmax - maximum uncertainty in wind velocity that is reported cc
cc              if uncertainty > errmax, wind velocity is not reported.cc
cc  images(1) - first FITS image of image pair. This image must be a  cc
cc              a lat-lon projection of the planet                    cc
cc  images(2) - second FITS image of image pair. This image must be a cc
```

```
cc              a lat-lon projection of the planet                      cc
cc      dtime - time interval between images 1 and 2 (seconds)          cc
cc                                                                      cc
cc    o u t p u t :                                                     cc
cc                                                                      cc
cc      xlat0 - latitude of box center for this output point            cc
cc      xlon0 - longitude of box center for this output point           cc
cc     latoff - latitude offset (pixels) from nominal alignment         cc
cc     lonoff - longitude offset (pixels) from nominal alignment        cc cc          u -
nominal zonal wind at best alignment (m/s)              cc
cc         du - error in u (m/s) estimated from half-width at half max cc
cc              of rms variations as function of longitude lag.         cc
cc          v - nominal meridional wind (m/s)                           cc
cc         du - error in v (m/s) estimated from half-width at half max cc
cc              of rms variations as function of latitude lag.          cc
cc                                                                      cc
ccccccccccccccccccccccccccccc  w i n d s  ccccccccccccccccccccccccccccc
c
      parameter (icol = 256, irow = 256, nim = 2)
      parameter (icolrow = 160000)
c
      character*80 hdr(36),imagename
      character*60 images(2)
      character*40 filout
      character*8 dellat,dellon
c
      integer iuim(2)
      integer*2 im0(icolrow),ibox1(icol,irow),ibox2(icol,irow)
      real*4 fimage(icol,irow,nim)
      real*4 ubin(irow),vbin(irow),dubin(irow),dvbin(irow)
      real*8 xlon(icol),xlat(irow),rms(icol,irow),box1(icol,irow),
     -       box2(icol,irow),boxdif(icol,irow),avgdif,box1avg,box2avg
c
c****   define io units
c
      iuout = 10
      iuim(1) = 8
      iuim(2) = 9
c
c*****   define pi and conversion from degrees to radians
c
      pi = acos(-1.0)
      dtr = pi/180.
c
c*****  read information about planet etc
c
      icut = 10
      write(*,*) 'enter effective radius of planet (km): '
      read(*,*) radkm
      radius = 1000.*radkm
      eqmdeg = 2.*pi*radius/360.
c
c****    enter output file name
c
      write(*,'(/,1a)') ' Enter the name of the output velocity file: '
      read(*,'(1a)') filout
c
c****   open output unit and write banner
c
      open(iuout,file=filout,form='formatted',status='unknown')
c
      write(*,'(6(/,1a))')
     - ' This program finds mean wind velocities for a specified ',
     - ' range of latitudes and longitudes by minimizing the ',
```

```
     - ' differences of contrast features within a rectangular ',
     - ' sample box with specified latitudes and longitude dimensions.',
     - ' Specify the latitude and longitude dimensions of feature ',
     - ' search box (deg): '
c
      read(*,*) wlon,wlat
c
      write(*,'(4(/,1a))')
     - ' The initial alignment of the master and test images is ',
     - ' determined for an initial guess of the rotation period. ',
     - ' Enter an initial guess for the rotation period (days): '
c
      read(*,*) perd
c
c****  convert period to seconds and compute nominal
c      equatorial zonal velocity
c
      per0 = 86400.*perd
      du0 = 2.*pi*radius/per0
      write(*,*) 'nominal equatorial wind = ',du0,' m/sec'
c
      write(*,'(4(/,1a))')
     - ' To align contrast features in the master image with those in ',
     - ' the test image, the test image is translated over a range ',
     - ' of latitudes and longitudes.  Enter the number of pixels to ',
     - ' translate the box in latitude and longitude: '
c
      read(*,*) nlon0,nlat0
c
      write(*,'(6(/,1a))')
     - ' When the test box is translated relative to the master box, ',
     - ' the number of valid overlapping points may be reduced ',
     - ' substantially.  If this number of points is too small, the  ',
     - ' fit will be meaningless.  Specify the minimum fraction of ',
     - ' the area of the two boxes the must include valid points: ',
     - ' for each relative position (0 - 1):'
c
      read(*,*) overlap
c
      write(*,'(6(/,1a))')
     - ' When the two images are aligned to minimimize the absolute ',
     - ' differences between the contrast features, this best fit ',
     - ' must account for a substantial fraction of the tolal ',
     - ' variance seen within the sample box. Specify the minimum ',
     - ' fraction of the variance that must be accounted for by the ',
     - ' best fit (0 - 1): '
c
      read(*,*) varmin
c
      write(*,'(5(/,1a))')
     - ' The program must determine if there are any significant ',
     - ' contrast features to track in each lat-lon box.  If the ',
     - ' box includes no contrast features, it is rejected. ',
     - ' Specify the minimum RMS contrast required ',
     - ' for this box to be used (0 - 1): '
c
      read(*,*) rmsbxmn
c
      write(*,'(3(/,1a))')
     - ' Box positions with large wind uncertainties are not reported.',
     - ' Enter maximum wind uncertainty that is reported (m/s):'
c
      read(*,*) errmax
c
```

```
c****   define number of output latitude and longitude boxes
c
      nlatbox = 180./(wlat)
      nlonbox = 360./(wlon)
c
      write(iuout,'(/,1a)')
     -   ' f e a t u r e - t r a c k e d   w i n d s :'
c
c****    read each image pair
c
      dellat = 'DEL LAT '
      dellon = 'DEL LON '
      nimage = 0
      im = 0
1003      write(*,'(/,2a,i5)')
     -     ' Enter the file name for the first of the',
     -     ' the two images in image pair: ',im+1
          read(*,'(1a)',end=6001) images(1)
c
          write(*,'(/,2a,i5)')
     -     ' Enter the file name for the second of the',
     -     ' the two images in image pair: ',im+1
          read(*,'(1a)',end=6001) images(2)
c
          write(*,'(/,1a,i5)')
     -     ' Enter the time interval between the two images (sec): '
          read(*,*,end=6001) dtime
          im = im + 1
c
c****       check to see if these files are available.
c
          open(iuim(1),file=images(1),status='old',access='direct',
     -          recl=2880,err=1021)
          close(iuim(1))
          open(iuim(2),file=images(2),status='old',access='direct',
     -          recl=2880,err=1041)
          close(iuim(2))
c
          go to 2001
1021      write(*,*) 'error: image file: ',images(1),' not found.'
          go to 1003
1041      write(*,*) 'error: header file: ',images(2),' not found.'
          go to 1003
c
2001      do 2421 n=1,2
c
c****            read the fits image
c
              imagename = images(1)
c
              call readfits(imagename,iuim(n),nx,ny,bzero,bscale,
     -                      im0,hdr,nrec_hdr)
c
              write(*,*) 'finished reading image # ',n
c
              call fitsheader(hdr,nrec_hdr,dellat,14,dlat)
        write(*,*) 'dlat = ',dlat
c
              call fitsheader(hdr,nrec_hdr,dellon,14,dlon)
        write(*,*) 'dlon = ',dlon
        if(dlat .eq. 0.0 .or. dlon .eq. 0.0) stop
c
c              re-stack the image into a 2-d array (array is read into
c              contiguous elements of a 1-d array).
```

```
c
              ict = 0
              if(bscale .eq. 0.) bscale = 1.
              do 2402 j=1,ny
                  do 2402 i=1,nx
                      ict = ict + 1
                      fimage(i,j,n) = bzero + bscale*im0(ict)
2402          continue
2421      continue
c
c****       create latitude and longitude arrays
c
          do 2041 ir=1,ny
              xlat(ir) = float(ir-1)*dlat - 90.
2041      continue
          do 2061 ic=1,nx
              xlon(ic) = float(ic-1)*dlon
2061      continue
c
c****       define the nomimal longitude offset between images 1 and 2.
c           the fraction of a rotation that has occurred between the
c           two observations is given by dtime/per0.  We then must
c           convert from degrees rotation (360 degrees/rotation) to
c           pixels by dividing by the number of degrees per pixel, dlon.
c
          nloff0 = 360.*dtime/(per0*dlon)
c
          nloff = nloff0
c
2081      if(nloff .gt. nx) then
c
c****         the pointer has been moved beyond the end of the array.
c             re-wrap the pointer to the begining of the array.
c
            write(*,*) 'nloff0 =',nloff0,
     -      ' offset pointer rapped back by nx'
            nloff = nloff - nx
            go to 2081
          endif
c
2091      if(nloff .lt. -nx) then
c
c*****        the pointer has been moved off the beginning of the
c             map.  move it to the far end of the map.
c
            write(*,*) 'nloff0 =',nloff0,
     -      ' offset pointer rapped forward by nx'
            nloff = nloff + nx
            go to 2091
          endif
c
c****        define the observation time offset in seconds
c
          hrs = dtime/3600.
c
c****        write out banner at the top of the output file.
c
          write(iuout,'(/,/,2a,/,2a)')
     -          '   image 1:          ',images(1),
     -          '   image 2:          ',images(2)
          write(iuout,'(1a,f10.1,1a)')     '   time difference:       ',
     -                                 hrs,' hours'
          write(iuout,'(1a,i5)')           '   nominal pixel offset: ',
     -                                 nloff
```

```
c
      write(iuout,'(/,3a,/,3a,/)')
     -   '   lon    lat  nlon nlat      u           du          ',
     -   'v           dv          rms',
     -   '           rms          rms          npix   ',
     -   '  (deg)   (deg)  pix  pix    (m/sec)      (m/sec) ',
     -   '    (m/sec)      (m/sec)     minimum     fraction  ',
     -   'difference     overlap'
c
c       define the number of points in each lat and lon box
c
      nlatb = wlat/dlat + 1
      nlonb = wlon/dlon + 1
      nlatb2 = nlatb/2
      nlonb2 = nlonb/2
      npixmax = nlonb*nlatb
c
c****   initialize output latitude bins for this image pair
c
      do 2801 nltb=1,2*nlatbox - 1
          ubin(nltb) = 0.0
          vbin(nltb) = 0.0
          dubin(nltb) = 0.0
          dvbin(nltb) = 0.0
2801  continue
c
c****   lat-lon box loop:   loop through each lat and lon box in
c       image number 1.  for each box position, offset image 2
c       and find the differece between images 1 and 2 in
c       the box.  use only valid (fimage > 0) points.  find the
c       offset that give the smallest rms difference.
c
      do 4221 nltb=1,2*nlatbox - 1
c
c****           define the latitude offset index and center of the box
c
          lat1 = (nltb - 1)*nlatb2
          xlat0 = xlat(lat1 + 1) + wlat/2.
c
          do 4208 nlnb=1,2.*nlonbox - 1
c
c****           define the longitude offset index and center of the box
c
              lon1 = (nlnb - 1)*nlonb2
              xlon0 = xlon(lon1 + 1) + wlon/2.0
c
c****            load image 1 box array.
c
              boxlavg = 0.
              npix = 0
              do 3041 lat=1,nlatb
                  lt1 = lat1 + lat
                  if(lt1 .lt. ny) then
                    do 3001 lon=1,nlonb
                        ln1 = lon1 + lon
                        if(ln1 .lt. nx) then
                          box1(lon,lat) =
     -                        fimage(ln1,lt1,1)
                          if(box1(lon,lat) .gt. 0.) then
                            ibox1(lon,lat) = 1
                            boxlavg = boxlavg + box1(lon,lat)
                            npix = npix + 1
                          else
                            ibox1(lon,lat) = 0
```

```
                              endif
                            else
                              box1(lon,lat) = 0.0
                              ibox1(lon,lat) = 0
                            endif
3001                      continue
                        else
                          do 3021 lon=1,nlonb
                             box1(lon,lat) = 0.0
                             ibox1(lon,lat) = 0
3021                      continue
                        endif
3041                continue
c
                    if(npix .ne. 0) then
                      box1avg = box1avg/npix
                    else
c                      write(*,*) ' there were no good points in box: ',
c     -                           nlnb,nltb
                      go to 4208
                    endif
c
c****                 find the rms of box 1
c
                    rmsbox1 = 0.0
                    do 3062 lat=1,nlatb
                        do 3062 lon=1,nlonb
                            if(ibox1(lon,lat) .gt. 0)
     -                          rmsbox1 = rmsbox1 + (box1(lon,lat) -
     -                                               box1avg)**2
3062                continue
c
                    rmsbox1 = sqrt(rmsbox1/npix)
c
c****                 determine if this box has any real structure
c
                    if(rmsbox1 .lt. rmsbxmn*box1avg) then
                      write(*,'(2a,1pe12.4,1a,1pe12.4,1a,1pe12.4)')
     -                ' RMS too small in box centered at ',
     -                'lon =',xlon0,'  lat =',xlat0, '  RMS =',rmsbox1
                      go to 4208
                    endif
c
c****                  i m a g e 2    l a t i t u d e    l a g    l o o p
c
                    npixmin = 0
                    rmsmin = 1.e30
                    rmsdif = -9999
                    latmin = 0
                    lonmin = 0
                    do 3821 llat=-nlat0,nlat0
c
c****                     find index offset of first pixel
c
                        nt0 = nlat0 + llat + 1
                        nt1 = lat1 + llat
c
c****                      i m a g e 2    l o n g i t u d e    l a g    l o o p
c
                        do 3802 llon=-nlon0,nlon0
c
                            nn0 = nlon0 + llon + 1
                            nn1 = lon1 + llon + nloff
c
```

```
c****                    load the offset box array for image 2
c
                        box2avg = 0.
                        npix = 0
                        do 3141 lat=1,nlatb
                            lt2 = nt1 + lat
                            if(lt2 .ge. 1 .and. lt2 .le. ny) then
                              do 3111 lon=1,nlonb
                                  ln2 = nn1 + lon
3102                              if(ln2 .gt. nx) then
                                    ln2 = ln2 - nx
                                    go to 3102
                                  endif
                                  if(ln2 .lt. 0) then
                                    ln2 = nx + ln2
                                    go to 3102
                                  endif
c
                                  box2(lon,lat) = fimage(ln2,lt2,2)
                                  if(box2(lon,lat) .gt. 0.) then
                                    ibox2(lon,lat) = 1
                                    box2avg = box2avg +
     -                                        box2(lon,lat)
                                    npix = npix + 1
                                  else
                                    ibox2(lon,lat) = 0
                                  endif
3111                            continue
                              else
                                do 3121 lon=1,nlonb
                                    box2(lon,lat) = 0.0
                                    ibox2(lon,lat) = 0
3121                            continue
                              endif
3141                    continue
                        if(npix .ne. 0) then
                          box2avg = box2avg/npix
                        else
c                          write(*,*) 'there were no good points in ',
c     -                               'box 2 for lag:',llon,llat
                          go to 3802
                        endif
c
c****                     find the point-by-point difference and mean
c                         difference between boxes 1 and 2
c
                        avgdif = 0.0
                        npix = 0
                        do 3202 lat=1,nlatb
                            do 3202 lon=1,nlonb
                              if(ibox1(lon,lat) .ne. 0 .and.
     -                           ibox2(lon,lat) .ne. 0) then
                                npix = npix + 1
                                boxdif(lon,lat) = (box2(lon,lat) -
     -                                             box2avg) -
     -                                            (box1(lon,lat) -
     -                                            box1avg)
                                avgdif =  avgdif + boxdif(lon,lat)
                              else
                                boxdif(lon,lat) = 0.
                              endif
3202                    continue
c
                        if(npix .gt. 0) then
```

```
                          avgdif = avgdif/npix
                        else
c                          write(*,*) 'there were no common points ',
c     -                               'in boxes 1&2 for lag:',llon,llat
                          avgdif = -999.
                          go to 3802
                        endif
c
c****                       find the rms difference between boxes 1 and 2
c
                        npix = 0
                        rms(nn0,nt0) = 0.0
                        do 3242 lat=1,nlatb
                            do 3242 lon=1,nlonb
                                if(ibox1(lon,lat) .ne. 0 .and.
     -                             ibox2(lon,lat) .ne. 0) then
                                  npix = npix + 1
                                  rms(nn0,nt0) = rms(nn0,nt0) +
     -                                           (boxdif(lon,lat) -
     -                                           avgdif)**2
                                endif
3242                        continue
c
                        rms(nn0,nt0) = sqrt(rms(nn0,nt0)/npix)
c
c****                       compare this rms to those for other lags.
c
                        if(npix .gt. overlap*npixmax) then
                          if(rms(nn0,nt0) .lt. rmsmin) then
                            npixmin = npix
                            rmsmin = rms(nn0,nt0)
                            latmin = llat
                            lonmin = llon
                          else
                            if(rms(nn0,nt0) .gt. rmsmax)
     -                        rmsmax = rms(nn0,nt0)
                          endif
                        else
                          rms(nn0,nt0) = 1.e30
                        endif
c
c****                       t r y   n e x t   l o n - l a g
c
3802                  continue
c
c****                    t r y   n e x t   l a t - l a g
c
3821                continue
c
c****                 estimate significance of best guess:
c                     (1) is the min rms at an extreme lag?
c                     (2) what fraction of the total variance within the
c                         boxes is accounted for?
c                     (3) are min and maxrms is significantly different?
c                     (4) how sharp is the feature?
c
                    if(latmin .le. -nlat0 .or. latmin .ge. nlat0) then
                      write(*,'(2a,1pe12.4,1a,1pe12.4,1a,i5)')
     -                ' Min rms found at latitude limit: ',
     -                ' lon =',xlon0,'  lat =',xlat0,' latmin =',latmin
                      go to 4208
                    endif
                    if(lonmin .le. -nlon0 .or. lonmin .ge. nlon0) then
                      write(*,'(2a,1pe12.4,1a,1pe12.4,1a,i10)')
```

```
     -              ' Minimum rms found at longitude limit: ',
     -              ' lon =',xlon0,'  lat =',xlat0,' lonmin = ',lonmin
                    go to 4208
                  endif
c
c****               compare the min variance to total rms of box 1:
c
                  if(rmsmin .gt. (1.0 - varmin)*rmsbox1) then
                    write(*,'(1a,1pe12.4,1a,1pe12.4,1a,1pe12.4)')
     -              ' Best fit accounts for < ',varmin,
     -              ' of rms at lon=',xlon0,' lat=',xlat0
                    go to 4208
                  endif
c
                  rmsfrac = 1.0 -  rmsmin/rmsbox1
c
c****               find relative difference between max and min rms
c
                  rmsdif = rmsmax - rmsmin
c
c****               determine "half-width" of rms best fit curve
c
                  dmean = 0.0
                  wgt = 0.0
                  drms0 = 0.2*rmsdif
                  do 4002 llat=-nlat0,nlat0
                      nt0 = nlat0 + llat + 1
                      y2 = (llat - latmin)**2
                      do 4002 llon=-nlon0,nlon0
                          nn0 = nlon0 + llon + 1
                          drms = rms(nn0,nt0) - rmsmin
                          if(drms .lt. drms0 .and.
     -                         rms(nn0,nt0) .ge. rmsmin) then
                            x2 = (llon - lonmin)**2
                            d2 = sqrt(x2 + y2)
                            dmean = dmean + d2
                            wgt = wgt + 1.
                          endif
4002              continue
c
                  if(wgt .ne. 0.0) then
                    dmean = dmean/wgt
                  else
                    dmean = 9999.
                  endif
c
c****                 compute the wind velocity corresponding to this lag
c
                  lonoff = lonmin + nloff0
c
                  if(lonoff .eq. 0) then
                    write(*,'(1a)') ' Unrealistic zero zonal wind: '
                    go to 4208
                  endif
c
                  latoff = latmin
                  u = lonoff*dlon*eqmdeg*cosd(xlat0)/dtime
                  v = 0.5*latmin*dlat*eqmdeg/dtime
c
c****                 compute the wind velocity rms from dmean
c
                  du = dmean*dlon*eqmdeg*cosd(xlat0)/dtime
                  dv = 0.5*dmean*dlat*eqmdeg/dtime
c
```

```
                  if(du .gt. errmax) then
                    write(*,*) 'mean error =',dmean,' pixels'
                    write(*,*) 'zonal wind uncertainty > ',
     -              'cutoff at lon=',xlon0,' lat=',
     -              xlat0, '  du =',du
                    go to 4208
                  endif
c
                  if(dv .gt. errmax) then
                    write(*,*) 'mean error =',dmean,' pixels'
                    write(*,*) 'meridioanl wind uncertainty > ',
     -              'cutoff at lon=',xlon0,' lat=',
     -              xlat0,'  dv = ',dv
                    go to 4208
                  endif
c
c****               print best-guess lon and lat lags and significance
c
                  write(iuout,'(2f7.1,2i5,7(1pe12.4),i10)')
     -              xlon0,xlat0,lonoff,latoff,u,du,v,dv,
     -              rmsmin,rmsfrac,rmsdif,npixmin
c
c****                   add values to appropriate output bins:
c
                  if(du .gt. 0.) then
                    ubin(nltb) = ubin(nltb) + u/(du*du)
                    dubin(nltb) = dubin(nltb) + 1./(du*du)
                  else
                    ubin(nltb) = ubin(nltb) + u
                    dubin(nltb) = dubin(nltb) + 1.
                  endif
                  if(dv .gt. 0.) then
                    vbin(nltb) = vbin(nltb) + v/(dv*dv)
                    dvbin(nltb) = dvbin(nltb) + 1./(dv*dv)
                  else
                    vbin(nltb) = vbin(nltb) + v
                    dvbin(nltb) = dvbin(nltb) + 1.
                  endif
c
c****               g e t    n e x t    l a t / l o n    b o x
c
4208            continue
4221        continue
c
c****         write out binned results:
c
            write(iuout,'(/,1a,/)')  ' b i n n e d    r e s u l t s :'
c
            write(iuout,'(1a,/,1a,/)')
     -        '   lat       u          du          v          dv',
     -        '  (deg)    (m/sec)     (m/sec)     (m/sec)     (m/sec)'
c
            do 5003 nltb=1,2*nlatbox-1
                lat1 = (nltb - 1)*nlatb2
                xlat0 = xlat(lat1 + 1) + wlat/2.
                if(dubin(nltb) .ne. 0.0) then
                  ubin(nltb) = ubin(nltb)/dubin(nltb)
                  dubin(nltb) = sqrt(1./dubin(nltb))
                else
                  go to 5003
                endif
                if(dvbin(nltb) .ne. 0.0) then
                  vbin(nltb) = vbin(nltb)/dvbin(nltb)
                  dvbin(nltb) = sqrt(1./dvbin(nltb))
```

```
              else
                go to 5003
              endif
c
              write(iuout,'(f7.1,7(1pe12.4))')
     -          xlat0,ubin(nltb),dubin(nltb),vbin(nltb),dvbin(nltb)
5003       continue
c
c****    g e t    n e x t    i m a g e     p a i r
c
      go to 1003
c
6001  close (iuout)
c
      stop
      end


      subroutine readfits(fitsfile,iuim,naxis1,naxis2,bzero,bscale,
     -                    im0,hdr,ir_hdr)
c
ccccccccccccccccccccccccc  r e a d f i t s  ccccccccccccccccccccccccc
cc                                                                   cc
cc    p u r p o s e:                                                 cc
cc                                                                   cc
cc    this subroutine reads a fits file in binary or i*2 format and  cc
cc    returns the values in this file as a integer*2 array.          cc
cc                                                                   cc
cc                                                                   cc
cc                                                                   cc
ccccccccccccccccccccccccc  r e a d f i t s  ccccccccccccccccccccccccc
c
c*****   define number of bytes in a fits record:
c
      parameter (irec = 2880, nbyte=512000)
c
      character*80 hdr(36),hdr_rec
      character*80 fitsfile
      character*8 name
      character*71 value
c
      logical simple
c
      byte byte0(nbyte),bytebuf4(4),bytebuf2(2)
c
      integer bitpix,naxis,naxis1,naxis2
      integer*2 i2buf,im0(nbyte)
      integer i4buf
c
      real bscale,bzero
c
      equivalence (bytebuf2,i2buf),(bytebuf4,i4buf)
c
c****       check to see if these files are available.
c
      write(*,'(1a,i5,5x,1a)') 'iuim,fitsfile  ',iuim,fitsfile
c
      close(iuim)
      open(iuim,file=fitsfile,status='old',access='direct',recl=irec)
c
c****   define end-of-header flag
c
      ihdr_end = 0
      ih = 0
```

```
      bscale = 1.0
      bzero = 0.0
c
c****   define a default unit for parsing header
c
      iuio = 3
      close(iuio)
      open(iuio,status='scratch',form='formatted')
c
c****    read the header
c
      ir = 0
1041  ir = ir + 1
      read(iuim,rec=ir,err=1061) hdr
c
      go to 2001
1061  write(*,*) 'error in record #', ir
c
c****    parse each header value
c
2001  ih = ih + 1
      hdr_rec = hdr(ih)
      name = hdr_rec(1:8)
      value = hdr_rec(10:80)
      rewind(iuio)
      if(name .eq. 'SIMPLE  ') then
        write(iuio,'(1a)') value
        rewind(iuio)
        read(iuio,*) simple
        write(*,*) 'simple= ',simple
      else
        if(name .eq. 'BITPIX  ') then
          write(iuio,'(1a)') value
          rewind(iuio)
          read(iuio,*) bitpix
          write(*,*) 'bitpix = ',bitpix
        else
          if(name .eq. 'NAXIS   ') then
            write(iuio,'(1a)') value
            rewind(iuio)
            read(iuio,*) naxis
            write(*,*) 'naxis = ',naxis
          else
            if(name .eq. 'NAXIS1  ') then
              write(iuio,'(1a)') value
              rewind(iuio)
              read(iuio,*) naxis1
              write(*,*) 'naxis1 = ',naxis1
            else
              if(name .eq. 'NAXIS2  ') then
                write(iuio,'(1a)') value
                rewind(iuio)
                read(iuio,*) naxis2
                write(*,*) 'naxis2 = ',naxis2
              else
                if(name .eq. 'BSCALE  ') then
                  write(iuio,'(1a)') value
                  rewind(iuio)
                  read(iuio,*) bscale
                  if(bscale .eq. 0.0) bscale = 1.0
                  write(*,*) 'bscale = ',bscale
                else
                  if(name .eq. 'BZERO   ') then
                    write(iuio,'(1a)') value
```

```
                    rewind(iuio)
                    read(iuio,*) bzero
                    write(*,*) 'bzero = ',bzero
                   else
                    if(name .eq. 'END     ') then
                      ihdr_end = 1
                      write(*,*) 'end of header: '
                      go to 3001
                    endif
                  endif
                endif
              endif
            endif
          endif
        endif
      endif
c
      if(ih .lt. 36) then
        go to 2001
      else
        go to 1041
      endif
c
3001  ir_hdr = ih
c
c****   define the total length of the input array:
c
      length = naxis1*naxis2*bitpix
c
c****    read the fits image
c
      i2 = 0
4001  ir = ir + 1
      i1 = i2 + 1
      i2 = i1 + irec - 1
      read(iuim,rec=ir,err=4061) (byte0(ii),ii=i1,i2)
c
      if(i2 .lt. length) go to 4001
c
c****  convert the image to i*2
c
4061  if(bitpix .eq. 8) then
c
c****     no problem - data is in byte format.
c
        do 4201 i=1,length
            im0(i) = byte0(i)
4201    continue
c
      else
c
c****    create an integer*2 variable from each pair of bytes
c
        nvalues = naxis1*naxis2
c
        if(bitpix .eq. 16) then
c
c*****      there are 2 bits per pixel
c
          if(simple) then
c
c****        stack bytes with low-byte high (IEEE)
c
            do 4221 i=1,nvalues
```

```
                ii = 2*(i - 1) + 1
c
                bytebuf2(1) = byte0(ii)
                bytebuf2(2) = byte0(ii+1)
c
                im0(i) = i2buf
4221          continue
c
            else
c
c****          stack bytes with high-byte high (Vax, IBM DOS)
c
              do 4241 i=1,nvalues
                ii = 2*(i - 1) + 1
c
                bytebuf2(1) = byte0(ii+1)
                bytebuf2(2) = byte0(ii)
c
                im0(i) = i2buf
4241          continue
            endif
          else
c
c******      there are 4 bits per pixel
c
            if(simple) then
c
c****          stack bytes with low-byte high (IEEE)
c
              do 4261 i=1,nvalues
                ii = 4*(i - 1) + 1
c
                bytebuf4(1) = byte0(ii)
                bytebuf4(2) = byte0(ii+1)
                bytebuf4(3) = byte0(ii+2)
                bytebuf4(4) = byte0(ii+3)
c
                im0(i) = i4buf
4261          continue
c
            else
c
c****          stack bytes with high-byte high (Vax, IBM DOS)
c
              do 4281 i=1,nvalues
                ii = 4*(i - 1) + 1
c
                bytebuf4(4) = byte0(ii)
                bytebuf4(3) = byte0(ii+1)
                bytebuf4(2) = byte0(ii+2)
                bytebuf4(1) = byte0(ii+3)
c
                im0(i) = i4buf
4281          continue
            endif
          endif
        endif
c
        close(iuim)
        close(iuio)
c
        return
        end
```

```
      subroutine fitsheader(hdr,nrec,item,itype,fitsvalue)
c
ccccccccccccccccccccccccc  f i t s h e a d e r  ccccccccccccccccccccccc
cc                                                                     cc
cc    p u r p o s e:                                                   cc
cc                                                                     cc
cc    this subroutine parses a fits header and returns the value of    cc
cc    a specified fits value.                                          cc
cc                                                                     cc
cc    i n p u t :                                                      cc
cc                                                                     cc
cc       hdr - 2880-byte character variable containing header          cc
cc      nrec - number of 80-column records in header                   cc
cc      item - character*8 specifying item desired from fits header    cc
cc     itype - fortran data type of item:                              cc
cc             1) character                                            cc
cc             2) i*2                                                  cc
cc             4) i*4                                                  cc
cc             14) real*4                                              cc
cc                                                                     cc
ccccccccccccccccccccccccc  f i t s h e a d e r  ccccccccccccccccccccccc
c
c*****   define number of bytes in a fits record:
c
      parameter (irec = 2880, nbyte=512000)
c
      character*80 hdr(nrec),hdr_rec
      character*8 name,item
      character*71 charval,value
c
      byte fitsvalue(71)
c
      integer int4val
c
      integer*2 int2val
      real realval
c
      write(*,*) 'nrec,itype,item',nrec,itype,item
        do 1 i=1,nrec
1       write(*,'(1a)') hdr(i)
c
c****   define end-of-header flag
c
      ihdr_end = 0
      ih = 0
c
c****   define a default unit for parsing header
c
      iuio = 3
      iubyt = 4
      close(iuio)
      open(iuio,status='scratch',form='formatted')
      close(iubyt)
      open(iubyt,status='scratch',form='unformatted')
c
c****    parse each header value
c
2001  ih = ih + 1
      hdr_rec = hdr(ih)
      name = hdr_rec(1:8)
      if(name .eq. item) then
c
c****      find the value of the header item:
c
```

```
        value = ' '
        do  2021 i=1,71
             j = i + 9
             if(hdr_rec(j:j) .eq. '/') go to 2041
             value(i:i) = hdr_rec(j:j)
2021    continue
c
2041    if(itype .eq. 1) then
c
c****       the output variable type is character
c           stack the value into a character variable:
c            - find number of leading blanck and any quotes
c
           nlb = 0
           do 2101 l=1,71
               if(value(l:l) .ne. ' ' .and. value(l:l) .ne. '"' .and.
     -            value(l:l) .ne. "'" ) go to 2121
               nlb = nlb + 1
2101       continue
c
2121       ich = 0
           do 2141 l=nlb+1,71
               if(value(l:l) .eq. '"' .or.
     -            value(l:l) .eq. "'" ) go to 2161
               charval(l-nlb:l-nlb) = value(l:l)
               ich = ich + 1
2141       continue
c
c****        write this value out to a dummy file, and read it back
c            in as type byte.
c
2161       rewind (iubyt)
           write(iubyt) (charval(l:l),l=1,ich)
           rewind (iubyt)
           read(iubyt) (fitsvalue(l),l=1,ich)
c
         else
           if(itype .eq. 2) then
c
c****         output data type is integer*2
c
             rewind(iuio)
             write(iuio,'(1a)') value
             rewind(iuio)
             read(iuio,*) int2val
c
c****        write this value out to a dummy file, and read it back
c            in as type byte.
c
             rewind (iubyt)
             write(iubyt) int2val
             rewind (iubyt)
             read(iubyt) (fitsvalue(l),l=1,2)
           else
             if(itype .eq. 4) then
c
c****           output data type is integer*4
c
               rewind(iuio)
               write(iuio,'(1a)') value
               rewind(iuio)
               read(iuio,*) int4val
c
c****            write this value out to a dummy file, and read it back
```

```
c               in as type byte.
c
              rewind (iubyt)
              write(iubyt) int4val
              rewind (iubyt)
              read(iubyt) (fitsvalue(l),l=1,4)
            else
c
c****         output data type is real*4
c
              rewind(iuio)
              write(iuio,'(1a)') value
              rewind(iuio)
              read(iuio,*) realval
c
c****           write this value out to a dummy file, and read it back
c               in as type byte.
c
              rewind (iubyt)
              write(iubyt) realval
              rewind (iubyt)
              read(iubyt) (fitsvalue(l),l=1,4)
            endif
          endif
        endif
c
        return
c
      endif
c
      if(ih .lt. nrec) go to 2001
c
      write(*,'(/,3a)')
     - 'Error: header item: ',item,' not found in header.'
      close(iuio)
c
      return
      end
..................................... make file
#
# this make file creates the program winds
#
FFLAGS = -g -c -C bounds
LFLAGS = -g -C

objs = winds.o fitsheader.o readfits.o

winds: $(objs)
        f77 $(LFLAGS) -o $@ $(objs)

winds.o: winds.f
        f77 $(FFLAGS) winds.f

fitsheader.o: fitsheader.f
        f77 $(FFLAGS) fitsheader.f

readfits.o: readfits.f
        f77 $(FFLAGS) readfits.f
..................................... sample run script

6100.                           radius of planet+atmosphere
test.out
20.,20.                         latitude and longitude limits of box
-6.                             nominal period (days)
```

```
7,4                             lat and lon scan range (pixels)
0.5                             min fractional are of box overlapped
0.2                             mininum fractional variance
0.05                            minimum rms contrast to define a feature
50.                             maximum wind error reported (m/s)
/data3/dc/venus/obs/latlon/w62103.fits
/data3/dc/venus/obs/latlon/w62012.fits
19970.                          time difference (sec)
/data3/dc/venus/obs/latlon/w62303.fits
/data3/dc/venus/obs/latlon/w62020.fits
37456.                          time difference (sec)
/data3/dc/venus/obs/latlon/w62020.fits
/data3/dc/venus/obs/latlon/w62001.fits
58320.                          time difference (sec)
/data3/dc/venus/obs/latlon/w62803.fits
/data3/dc/venus/obs/latlon/w22003.fits
41759.                          time difference (sec)

.................................................sample output

  f e a t u r e - t r a c k e d   w i n d s :


   image 1:          /data3/dc/venus/obs/latlon/w62103.fits
   image 2:          /data3/dc/venus/obs/latlon/w62012.fits
   time difference:              5.5 hours
   nominal pixel offset:    -6

   lon    lat  nlon nlat      u          du          v          dv          rms          r
ms          rms          npix
  (deg)  (deg)  pix  pix   (m/sec)     (m/sec)     (m/sec)     (m/sec)     minimum      fra
ction  difference     overlap


 b i n n e d   r e s u l t s :

   lat      u          du          v          dv
  (deg)   (m/sec)     (m/sec)     (m/sec)     (m/sec)



   image 1:          /data3/dc/venus/obs/latlon/w62303.fits
   image 2:          /data3/dc/venus/obs/latlon/w62020.fits
   time difference:             10.4 hours
   nominal pixel offset:   -13

   lon    lat  nlon nlat      u          du          v          dv          rms          r
ms          rms          npix
  (deg)  (deg)  pix  pix   (m/sec)     (m/sec)     (m/sec)     (m/sec)     minimum      fra
ction  difference     overlap

   40.0  -50.0   -9    1 -3.2887E+01  1.0150E+01  2.8424E+00  7.8956E+00  6.9808E+02  6.96
32E-01  1.4721E+04        64
   80.0  -30.0  -13   -1 -6.4001E+01  2.3558E+01 -2.8424E+00  1.3601E+01  6.8017E+02  4.81
65E-01  1.4739E+04       121
   30.0  -20.0  -15   -1 -8.0130E+01  2.9894E+01 -2.8424E+00  1.5906E+01  1.3300E+03  2.14
55E-01  1.4089E+04        63
   80.0  -20.0  -10   -1 -5.3420E+01  2.8385E+01 -2.8424E+00  1.5103E+01  9.2547E+02  4.89
35E-01  1.4493E+04       121
   90.0  -20.0  -16   -2 -8.5472E+01  2.9912E+01 -5.6848E+00  1.5916E+01  7.5408E+02  4.61
44E-01  1.4665E+04        78
   30.0  -10.0  -15   -1 -8.3977E+01  2.6379E+01 -2.8424E+00  1.3393E+01  1.0654E+03  5.36
36E-01  1.4353E+04        67
   40.0  -10.0  -19   -1 -1.0637E+02  3.8202E+01 -2.8424E+00  1.9396E+01  1.0710E+03  2.89
```

28E-01 1.4348E+04 78
60.0 10.0 -8 2 -4.4788E+01 2.4825E+01 5.6848E+00 1.2604E+01 6.6617E+02 3.82
37E-01 1.4753E+04 121
70.0 10.0 -15 3 -8.3977E+01 3.1891E+01 8.5272E+00 1.6191E+01 7.2900E+02 2.30
88E-01 1.4690E+04 121
20.0 20.0 -10 2 -5.3420E+01 1.3284E+01 5.6848E+00 7.0685E+00 3.4211E+03 4.04
31E-01 1.1998E+04 66
70.0 20.0 -19 3 -1.0150E+02 4.0867E+01 8.5272E+00 2.1745E+01 9.0353E+02 4.90
29E-01 1.4515E+04 121
80.0 30.0 -9 -2 -4.4309E+01 2.9687E+01 -5.6848E+00 1.7140E+01 7.7833E+02 5.77
52E-01 1.4640E+04 96
30.0 50.0 -7 0 -2.5579E+01 1.1450E+01 0.0000E+00 8.9065E+00 8.5231E+02 5.46
37E-01 1.4566E+04 69
40.0 50.0 -14 -1 -5.1158E+01 1.7687E+01 -2.8424E+00 1.3758E+01 8.9052E+02 2.83
90E-01 1.4528E+04 65

b i n n e d r e s u l t s :

lat (deg)	u (m/sec)	du (m/sec)	v (m/sec)	dv (m/sec)
-50.0	-3.2887E+01	1.0150E+01	2.8424E+00	7.8956E+00
-30.0	-6.4001E+01	2.3558E+01	-2.8424E+00	1.3601E+01
-20.0	-7.2314E+01	1.6957E+01	-3.7558E+00	9.0226E+00
-10.0	-9.1207E+01	2.1707E+01	-2.8424E+00	1.1021E+01
10.0	-5.9575E+01	1.9590E+01	6.7573E+00	9.9459E+00
20.0	-5.8015E+01	1.2634E+01	5.9565E+00	6.7223E+00
30.0	-4.4309E+01	2.9687E+01	-5.6848E+00	1.7140E+01
50.0	-3.3133E+01	9.6117E+00	-8.3942E-01	7.4766E+00

image 1: /data3/dc/venus/obs/latlon/w62020.fits
image 2: /data3/dc/venus/obs/latlon/w62001.fits
time difference: 16.2 hours
nominal pixel offset: -20

lon (deg)	lat (deg)	nlon pix	nlat pix	u (m/sec)	du (m/sec)	v (m/sec)	dv (m/sec)	rms minimum	r ms fra ction
	rms difference		npix overlap						
30.0	-50.0	-19	3	-4.4590E+01	1.1420E+01	5.4766E+00	8.8832E+00	9.0999E+02	4.71
92E-01	1.4509E+04		61						
40.0	-50.0	-24	3	-5.6325E+01	1.7568E+01	5.4766E+00	1.3665E+01	1.0738E+03	2.50
37E-01	1.4345E+04		61						
70.0	-30.0	-19	-1	-6.0076E+01	1.5330E+01	-1.8255E+00	8.8510E+00	1.0747E+03	2.19
04E-01	1.4344E+04		121						
80.0	-30.0	-22	-1	-6.9562E+01	1.5930E+01	-1.8255E+00	9.1972E+00	8.9914E+02	3.43
34E-01	1.4520E+04		119						
90.0	-30.0	-22	-2	-6.9562E+01	1.6603E+01	-3.6511E+00	9.5856E+00	8.9516E+02	2.88
44E-01	1.4524E+04		64						
30.0	-20.0	-20	-3	-6.8618E+01	1.8126E+01	-5.4766E+00	9.6448E+00	9.7358E+02	2.46
82E-01	1.4445E+04		66						
70.0	-20.0	-22	-2	-7.5479E+01	1.8015E+01	-3.6511E+00	9.5856E+00	1.1251E+03	2.92
54E-01	1.4294E+04		121						
80.0	-20.0	-23	-2	-7.8910E+01	1.9069E+01	-3.6511E+00	1.0146E+01	9.7514E+02	2.95
34E-01	1.4444E+04		115						
60.0	-10.0	-19	3	-6.8316E+01	1.9706E+01	5.4766E+00	1.0005E+01	1.7902E+03	2.55
70E-01	1.3629E+04		121						
70.0	-10.0	-23	-3	-8.2699E+01	2.1585E+01	-5.4766E+00	1.0959E+01	1.3728E+03	3.26
32E-01	1.4046E+04		121						
80.0	-10.0	-24	-2	-8.6294E+01	2.1521E+01	-3.6511E+00	1.0927E+01	1.1093E+03	2.08
86E-01	1.4310E+04		110						
60.0	0.0	-20	3	-7.3021E+01	1.8157E+01	5.4766E+00	9.0787E+00	1.1961E+03	5.77

```
50E-01  1.4223E+04       121
   80.0     0.0  -21     3 -7.6672E+01  2.0010E+01  5.4766E+00  1.0005E+01  1.1729E+03  3.16
91E-01  1.4246E+04       107
   60.0    20.0  -26     3 -8.9203E+01  2.6090E+01  5.4766E+00  1.3882E+01  1.1291E+03  2.70
14E-01  1.4290E+04       110
```

b i n n e d r e s u l t s :

lat (deg)	u (m/sec)	du (m/sec)	v (m/sec)	dv (m/sec)
-50.0	-4.8076E+01	9.5748E+00	5.4766E+00	7.4479E+00
-30.0	-6.6148E+01	9.1966E+00	-2.3857E+00	5.3097E+00
-20.0	-7.4189E+01	1.0615E+01	-4.2771E+00	5.6481E+00
-10.0	-7.8444E+01	1.2056E+01	-8.0451E-01	6.1208E+00
0.0	-7.4670E+01	1.3447E+01	5.4766E+00	6.7234E+00
20.0	-8.9203E+01	2.6090E+01	5.4766E+00	1.3882E+01

image 1: /data3/dc/venus/obs/latlon/w62803.fits
image 2: /data3/dc/venus/obs/latlon/w22003.fits
time difference: 11.6 hours
nominal pixel offset: -14

lon (deg)	lat (deg)	nlon pix	nlat pix	u (m/sec)	du (m/sec)	v (m/sec)	dv (m/sec)	rms minimum	r ms fra ction	rms difference	npix overlap
40.0	-40.0	-9	-1	-3.5155E+01	1.3209E+01	-2.5495E+00	8.6216E+00	1.7056E+03	7.16	48E-01	1.3713E+04 109
50.0	-30.0	-14	-3	-6.1822E+01	2.1781E+01	-7.6485E+00	1.2575E+01	1.3173E+03	3.23	17E-01	1.4101E+04 121
60.0	-30.0	-18	-3	-7.9486E+01	2.8556E+01	-7.6485E+00	1.6487E+01	1.8606E+03	3.57	63E-01	1.3558E+04 121
20.0	-20.0	-8	0	-3.8332E+01	1.0406E+01	0.0000E+00	5.5369E+00	2.1729E+03	2.70	60E-01	1.3246E+04 68
30.0	0.0	-13	2	-6.6287E+01	2.3075E+01	5.0990E+00	1.1538E+01	1.7477E+03	2.09	63E-01	1.3671E+04 69
40.0	0.0	-18	1	-9.1782E+01	3.1188E+01	2.5495E+00	1.5594E+01	1.6469E+03	3.87	22E-01	1.3772E+04 69
60.0	0.0	-14	-3	-7.1386E+01	2.5675E+01	-7.6485E+00	1.2837E+01	1.5333E+03	2.70	00E-01	1.3886E+04 121
40.0	20.0	-8	3	-3.8332E+01	2.0695E+01	7.6485E+00	1.1012E+01	2.0934E+03	3.64	20E-01	1.3325E+04 121
20.0	30.0	-8	1	-3.5327E+01	7.5301E+00	2.5495E+00	4.3475E+00	1.9431E+03	4.27	94E-01	1.3476E+04 70

b i n n e d r e s u l t s :

lat (deg)	u (m/sec)	du (m/sec)	v (m/sec)	dv (m/sec)
-40.0	-3.5155E+01	1.3209E+01	-2.5495E+00	8.6216E+00
-30.0	-6.8319E+01	1.7318E+01	-7.6485E+00	9.9987E+00
-20.0	-3.8332E+01	1.0406E+01	0.0000E+00	5.5369E+00
0.0	-7.3962E+01	1.5036E+01	1.3443E-01	7.5181E+00
20.0	-3.8332E+01	2.0695E+01	7.6485E+00	1.1012E+01
30.0	-3.5327E+01	7.5301E+00	2.5495E+00	4.3475E+00